Positive Science International (PSI)

e-ISNN: 3108-3862

Volume 2 / Number 1
2026

SINOP UNIVERSITY PUBLICATIONS

POSITIVE SCIENCE INTERNATIONAL JOURNAL

PSI: Positive Science International

e-ISSN: 3108-3862

Volume: 2 Issue: 1 Year: 2026

POSITIVE SCIENCE INTERNATIONAL JOURNAL

Volume: 2 Issue: 1 Year: 2026

Publication Type

Periodical

Publisher

Sinop University

Faculty of Engineering and Architecture

Prof. Dr. Şakir TAŞDEMİR

Rector

Reviewers on This Issue

Positive Science International Journal uses a double-blind peer review system. Reviewer names are kept confidential and are not published.

Technical Editors

Instructor Yakup İRİM

Res. Assist. Fatih AKTÜRK

Language Editor

Instructor Yeliz YAZICI DEMİR

Layout Editors

Res. Assist. Dr. Nilay BİLGİN SARITAŞ

Res. Assist. Eda ALTUNTAŞ

Positive Science International Journal is an interdisciplinary peer-reviewed scientific journal established in 2024 by Sinop University Faculty of Engineering and Architecture, covering basic engineering and science topics. The journal is published electronically in 2 issues per year **(June and December).** Original "Research Articles" and "Reviews" in **English** are accepted by Positive Science International.

Contact

Faculty of Engineering and Architecture

Osmaniye Mahallesi Selanik Caddesi (Kuzey Kampüs) No: 52K 57000 - SİNOP

Tel: 0368 271 41 51 Fax: 0368 271 41 52

https://dergipark.org.tr/en/pub/psi

psi@sinop.edu.tr

CONTENT

Articles

C. Ganesa MOORTHY, G. Udhaya SANKAR **Research Article**

Architecture of Geometrical Construction for Multistage Thermoelectric System

Çok Aşamalı Termoelektrik Sistem için Geometrik Yapı Tasarımı 1-11

Oğuz Gürkan GÜDER, Sait Ozan YILMAZ, Sertaç EROL **Research Article**

Design and Analysis of Detachable Bolt Head (Zinc-Cap) From Zinc-Aluminum Series Alloys

ZA Serisinden Ayrılabilir Cıvata Başlığı (Zinc-Cap) Tasarımı ve Analizi 12-26

Adewole SEBIOMO **Research Article**

Microbial Analysis, Physicochemical Content and Insect Vectors Associated with Selected Dumpsites in Ijebu-Ode, Nigeria

Nijerya'nın Ijebu-Ode Bölgesinde Seçilmiş Çöp Depolama Alanlarıyla İlişkili Mikrobiyal Analiz, Fizikokimyasal Bileşim ve Böcek Vektörleri 27-42

Mertcan TUTUM, Yavuz ÜNAL **Research Article**

Evaluation of Kernel and Parameter Effects on the Performance of Classifiers for Differentiated Thyroid Cancer Recurrence

Farklılaşmış Tiroid Kanseri Nüksü İçin Sınıflandırıcıların Performansı Üzerindeki Çekirdek ve Parametre Etkilerinin Değerlendirilmesi 43-52

Erhan SESLİ **Review Article**

The Role of Wireless Sensor Networks in Military Operations: A Survey

Askeri Operasyonlarda Kablosuz Sensör Ağlarının Rolü: Bir Araştırma 53-71

Sinop University
Positive Science International
e-ISSN: 3108-3862

Positive Science International, 2(1), 1-11
Research Article, Year: 2026
DOI: 10.71340/psi.1856714

Architecture of Geometrical Construction for Multistage Thermoelectric System

C. Ganesa MOORTHY[1*], G. Udhaya SANKAR[2]

[1*] *Department of Mathematics, Alagappa University, Karaikudi – 630003, Tamilnadu, India.*

[2] *Independent Researcher, Karaikudi-630002, Tamilnadu, India.*

Article Info

Research article
Received: *05.01.2026*
Accepted: *23.02.2026*
Published: *30.06.2026*
***Corresponding Author*:** *C. Ganesa MOORTHY*
gmoorthyc@alagappauniversity.ac.in
0000-0003-3119-7531
Keywords

Geometry of Thermoelectric system, Energy application, cooling system.

Abstract

An architectural framework for a multistage thermoelectric system is developed by using COMSOL Multiphysics. The geometrical construction of the basic building blocks comprising Bi_2Te_3 material based p-type and n-type thermoelectric legs integrated with copper and tungsten thermocouples is systematically modeled and analyzed. A three dimensional multistage configuration is designed by a series-connected p-type and n-type legs arranged in layered segments. The influence of geometrical parameters and thermocouple architecture on system performance is evaluated through numerical simulations. The performance of the thermoelectric system is assessed in terms of coefficient of performance under different temperature differences and input currents. Simulation results demonstrate that the proposed multistage geometrical architecture achieves a maximum temperature difference of approximately 73.543 K and exhibits improved coefficient of performance at lower temperature gradients. The findings highlight the importance of geometrical construction and multistage architecture in enhancing thermoelectric system performance, providing useful design guidelines for efficient thermoelectric cooling and energy conversion applications.

Çok Aşamalı Termoelektrik Sistem için Geometrik Yapı Tasarımı

Makale Bilgisi

Araştırma makalesi
Başvuru: *05.01.2026*
Kabul: *23.02.2026*
Yayın: *30.06.2026*
***Sorumlu Yazar*:**
C. Ganesa MOORTHY
gmoorthyc@alagappauniversity.ac.in
0000-0003-3119-7531
Anahtar Kelimeler

Termoelektrik sistem geometrisi, enerji uygulamaları, soğutma sistemi

Özet

COMSOL Multiphysics kullanılarak çok kademeli bir termoelektrik sistem için mimari bir çerçeve geliştirilmiştir. Bi_2Te_3 malzemesine dayalı p-tipi ve n-tipi termoelektrik bacaklardan oluşan ve bakır ve tungsten termokupllarla entegre edilmiş temel yapı taşlarının geometrik yapısı sistematik olarak modellenmiş ve analiz edilmiştir. Üç boyutlu çok kademeli bir konfigürasyon, katmanlı segmentler halinde düzenlenmiş seri bağlı p-tipi ve n-tipi bacaklardan tasarlanmıştır. Geometrik parametrelerin ve termokupl mimarisinin sistem performansı üzerindeki etkisi sayısal simülasyonlar yoluyla değerlendirilmiştir. Termoelektrik sistemin performansı, farklı sıcaklık farkları ve giriş akımları altında performans katsayısı açısından değerlendirilmiştir. Simülasyon sonuçları, önerilen çok kademeli geometrik mimarinin yaklaşık 73.543 K' lik maksimum sıcaklık farkına ulaştığını ve daha düşük sıcaklık gradyanlarında iyileştirilmiş performans katsayısı sergilediğini göstermektedir. Bulgular, termoelektrik sistem performansını artırmada geometrik yapının ve çok aşamalı mimarinin önemini vurgulayarak, verimli termoelektrik soğutma ve enerji dönüştürme uygulamaları için faydalı tasarım kılavuzları sunmaktadır.

To cite this article:
Moorthy, G. C., Sankar, U. B. (2026). Architecture of Geometrical Construction for Multistage Thermoelectric, Positive Science International, 2(1), 1-11, https://doi.org/10.71340/psi.1856714

PSI
POSITIVE SCIENCE INTERNATIONAL
Research Article

1. Introduction

Thermoelectric systems are promising solid state devices for converting waste heat into electrical energy, especially in cool and medium temperature industrial applications [11]. However, their efficiency is limited because thermoelectric material properties vary with temperature, leading to mismatches in optimal operating conditions along the device length [13]. Segmented and functionally graded thermoelectric designs can improve performance by using different materials across temperature ranges, but their efficiency is still constrained by compatibility factor mismatches [12, 14]. Wu, Y. et al. [14] proposes a geometry optimization approach that adjusts the cross sectional area and thickness of thermoelectric elements to match the local compatibility factor at every segment. By fully utilizing existing thermoelectric materials and enabling fabrication through additive manufacturing techniques such as selective laser melting, the proposed method significantly enhances thermoelectric system efficiency and offers a practical pathway for high performance waste heat recovery systems [9, 10].

Li, et al. [5] provides a clear and comprehensive review of computational methods for designing geometry engineered thermoelectric devices. By shifting the focus from material only optimization to device level geometric engineering, they highlight how tailored leg geometries can significantly enhance thermoelectric performance, reliability, and thermal management. The review systematically covers fundamental principles, numerical modeling techniques, and modern optimization strategies including gradient based methods, and machine learning assisted approaches. The work offers a timely and valuable perspective on how advanced computational frameworks can accelerate the development of high performance thermoelectric devices [2, 7, 8]. Luo and Cheng [6] numerically investigated the geometry optimization of segmented asymmetrical thermoelectric system for waste heat recovery applications. Using three dimensional finite element simulations in COMSOL Multiphysics, they compared segmented pyramidal and segmented cone thermoelectric systems composed of Bi_2Te_3 and $CoSb_3$ legs operating in different temperature ranges. Their study examined the influence of segment height ratio, leg geometry, and hot side temperature on electrical output and thermal stress. Their results showed that an optimized segment height ratio significantly enhances electrical performance while reducing thermal stress, thereby improving device reliability. Although both geometries exhibited similar electrical performance due to identical volume and cross-sectional area, the cone shaped legs produced a more uniform thermal stress distribution, reducing the maximum von Mises stress by approximately 10% compared to pyramidal legs. This work demonstrates that combining segmentation with asymmetrical geometry is an effective strategy for simultaneously improving thermoelectric performance and mechanical reliability.

Li, et al. [4] presents a comparative numerical investigation of optimum thermoelectric element geometry in hybrid photovoltaic thermoelectric systems and standalone solar thermoelectric systems. By using a three dimensional finite element model implemented in COMSOL Multiphysics, the performance of hybrid photovoltaic thermoelectric systems devices integrated with two different

photovoltaic cell types is analyzed and compared with that of a standalone solar thermoelectric system under identical operating conditions. Rectangular and trapezoidal thermoelectric leg geometries are evaluated to determine their influence on power output and overall system efficiency. The results demonstrate that the optimum thermoelectric geometry strongly depends on the characteristics of the photovoltaic cell and differs from that of a standalone solar thermoelectric system, even under the same solar irradiation and concentration ratios. While trapezoidal legs can enhance performance in certain configurations, they are not universally optimal for all hybrid photovoltaic thermoelectric systems. The geometry optimization strategies developed for standalone solar thermoelectric systems cannot be directly applied to hybrid photovoltaic thermoelectric systems devices but they provide important design guidelines for geometry based optimization of hybrid solar energy systems. However, their widespread use is limited by relatively low conversion efficiency. One effective approach to improving thermoelectric system performance is geometry optimization of thermoelectric legs, which strongly influences temperature distribution, electrical resistance, heat flow, and thermal stress [1]. The numerical modeling and simulation are carried out to evaluate the performance of thermoelectric systems with different leg geometries under identical boundary conditions. By using effective material properties, thermoelectric system with square, circular, and trapezoidal leg cross sections are analyzed to investigate the effects of leg shape, cross sectional area, and length on power output, efficiency, junction temperatures, and thermal stress [3]. Kondaguli and Malaji [3] results indicate that trapezoidal leg geometries provide higher conversion efficiency, while square and circular cross sections yield higher power output. It highlights the importance of geometrical construction optimization as a practical strategy for enhancing thermoelectric system performance. Similarly, Ferreira and Pereira [1] conducted a systematic numerical investigation on the geometrical optimization of thermoelectric devices by using finite element simulations implemented in COMSOL Multiphysics. Their study examined thermocouples composed of Bi_2Te_3 p-type legs and n-type legs with copper electrical contacts, focusing on the influence of leg geometry, contact dimensions, and device configuration on electrical output. They demonstrated that cubic and cylindrical leg geometries with identical length and cross sectional area exhibit equivalent performance, indicating that device efficiency depends primarily on geometrical ratios rather than leg shape. An optimal height to width ratio of approximately (5×10^{-3}) was identified for maximizing power output, independent of the applied temperature gradient. Furthermore, their study showed that increasing the leg cross section enhances power generation, while contact resistance plays a critical role in performance, with optimal ratios found between contact height and leg height (~40) and contact length and leg width (<0.05). They reported that power output scales with the square of both the temperature difference and the number of thermocouples, highlighting the importance of device level geometric optimization alongside material selection. Hence that work provides valuable design guidelines for geometry driven performance enhancement of thermoelectric system.

The present work focuses on the geometrical construction of the basic building blocks of a p-type and n-type thermoelectric system by using COMSOL Multiphysics. The influence of copper

thermocouples on Bi_2Te_3 material based p-type and n-type thermoelectric legs are examined. Furthermore, the architecture of a multistage thermoelectric system is evaluated in terms of its coefficient of performance with respect to the temperature difference.

2. Architectural Framework

Software such as MATLAB is used to solve technical problems related to the design of thermoelectric systems through programming [2]. However, structural analysis is only partially possible in MATLAB. In contrast, COMSOL Multiphysics enables the creation of well-defined and detailed geometrical structures by applying appropriate parameters in the simulation settings [1, 5, 15-18]. In this work, COMSOL Multiphysics software is employed to develop the architectural framework of a thermoelectric system. The authors constructed a basic building block as a three dimensional unit consisting of both p-type and n-type frameworks. The p-type and n-type thermoelectric legs are distinct and include copper thermocouples attached to the top and bottom of each leg. The basic building block of the architectural framework is shown in Figure 1. The multistage thermoelectric system consists of a limited number of p-type and n-type thermoelectric leg materials connected in series in each segment. The construction of the multistage building block requires the formation of geometric layers of both p-type and n-type materials.

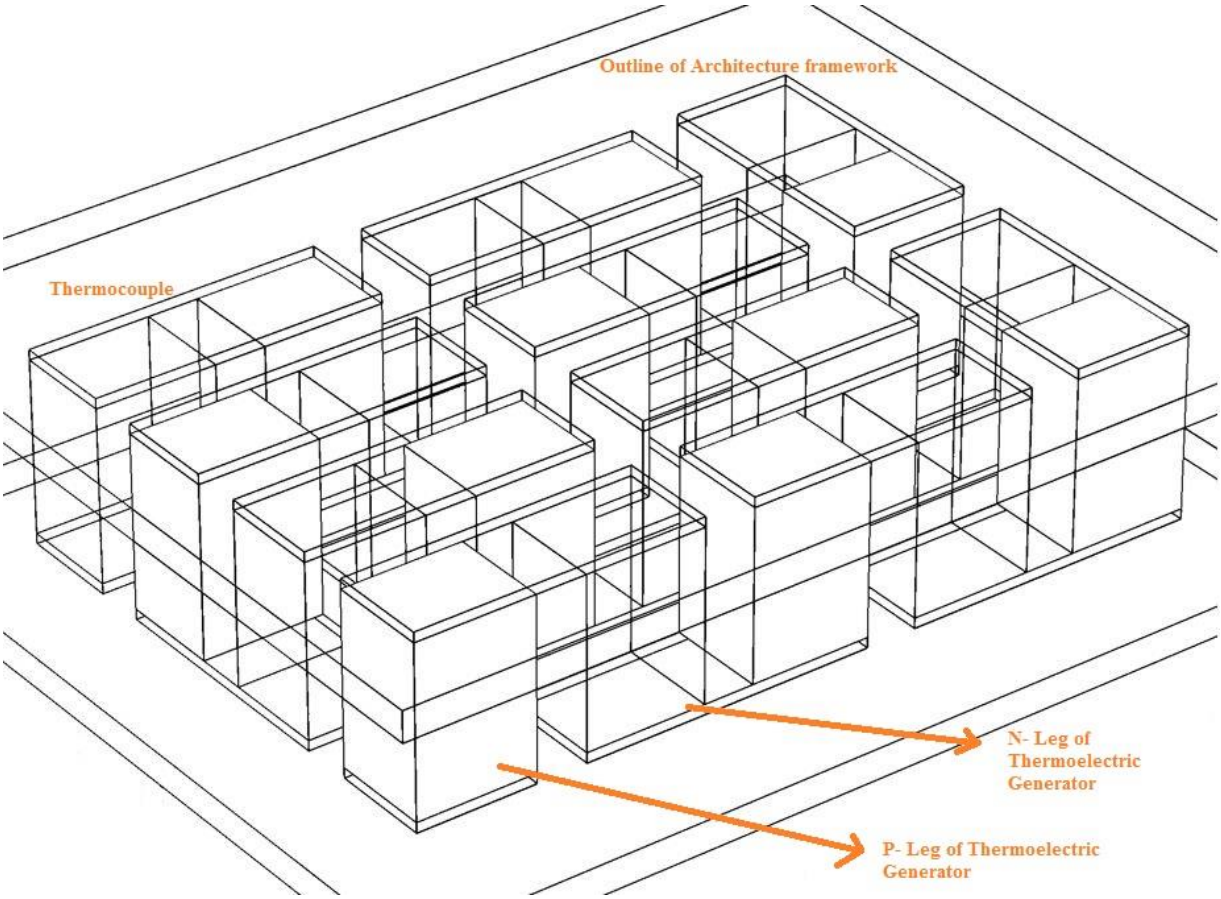

Figure 1. Architecture framework of multistage thermoelectric system

2.1. p-type Geometrical Construction

The p-type thermoelectric legs are constructed by using COMSOL Multiphysics. The p-type material leg is positioned within the basic building block of the Geometrical Construction framework, as shown in Figure 2. The leg materials are selected from the COMSOL material library [5, 16]. The corresponding thermocouples are placed above and below the thermoelectric legs. Multiple legs are added within the specified region, as described in Table 1. The parameters table assists in defining the architecture of the multistage p-type thermoelectric legs in the thermoelectric system.

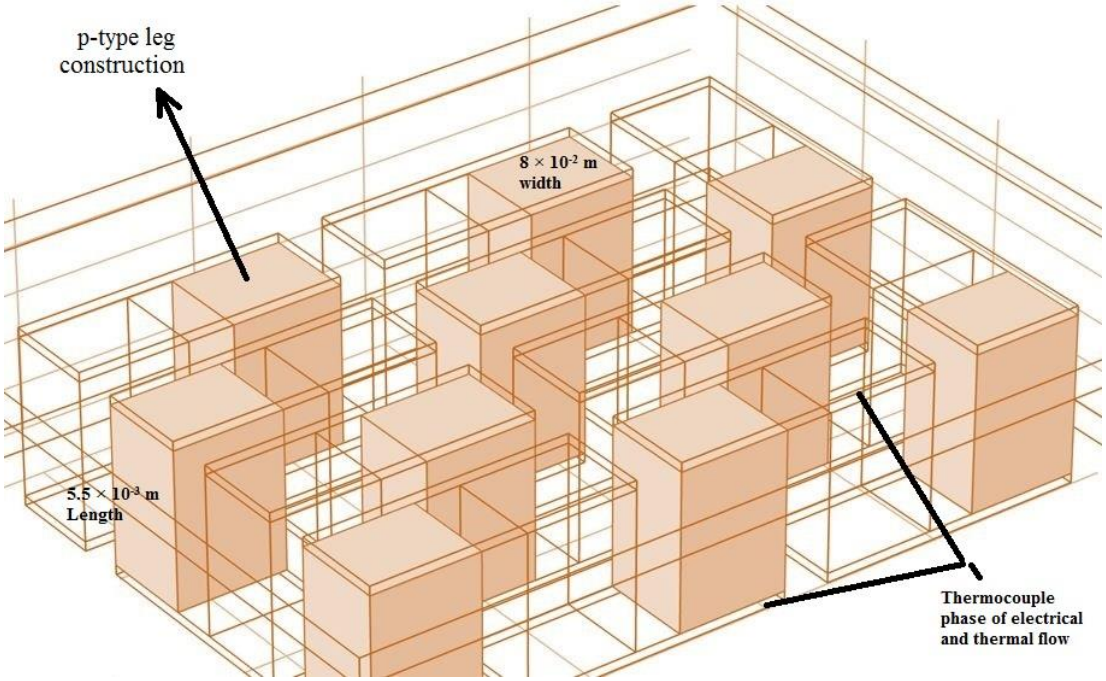

Figure 2. p-type Geometrical construction of thermoelectric system

Table 1. Parameters and values for geometry construction

Name of the parameters	Values
Length	8×10^{-3} m
Width	1×10^{-1} m
Height	2.5×10^{-3} m
Thickness of conductor	1×10^{-4} m
Thickness of ceramics	3×10^{-4} m
Cross section in leg length	1×10^{-3} m
Cross section in leg width	1.2×10^{-3} m
Leg height	1.7×10^{-3} m
Pitch	5×10^{-4} m
Length legs	4
Width legs	5
Length of legs	5.5×10^{-3} m
Width of legs	8×10^{-2} m
Thermocouples number	Maximum. 10

2.2. n-type Geometrical Construction

The n-type thermoelectric legs are modeled using COMSOL Multiphysics software. Each n-type leg is incorporated in the basic geometrical construction framework, as illustrated in Figure 3. The material properties of the n-type legs are assigned from the COMSOL material library. Thermocouples are attached to the upper and lower surfaces of the thermoelectric legs. A specified number of n-type legs are arranged within the designated region, as detailed in Table 1. The parameters table is used to configure and define the structural architecture of the multistage n-type thermoelectric legs in the thermoelectric system.

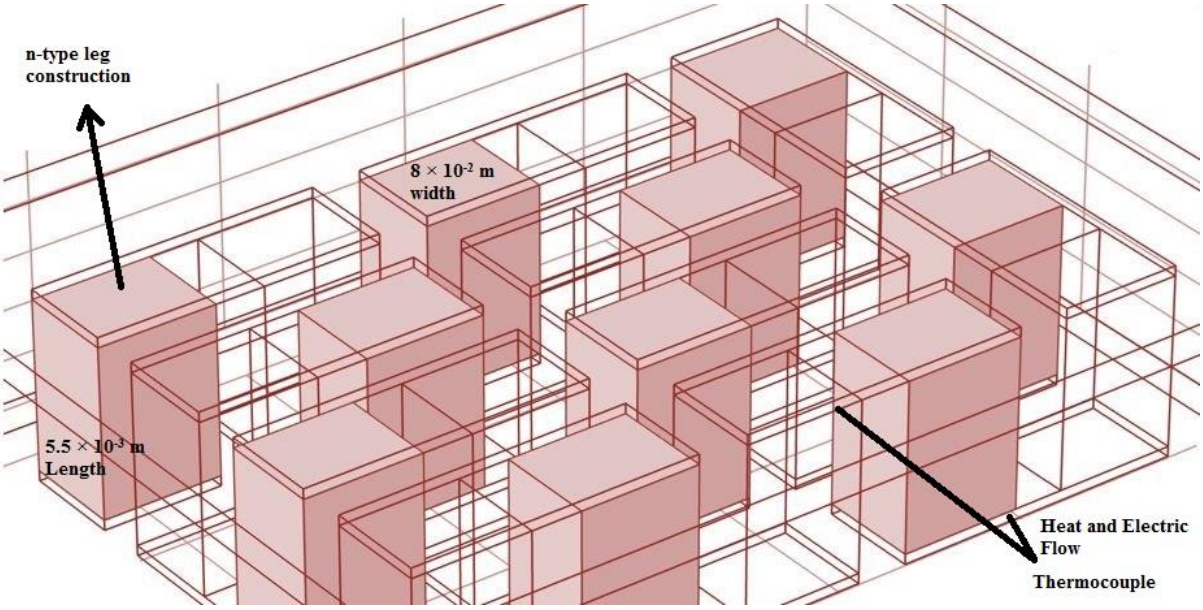

Figure 3. n-type Geometrical construction of thermoelectric system

2.3. Thermocouple Architectural Arrangement

The p-type and n-type thermoelectric legs are arranged in series, as illustrated in the geometrical construction. Figure 4 presents a holder-type architecture developed in COMSOL Multiphysics for positioning the p-type and n-type materials. The combined arrangement of both p-type and n-type legs forms the complete thermoelectric system. Copper thermocouples are used as holding and electrical connection elements for the p-type and n-type thermoelectric legs. In addition, the architectural performance can be further enhanced by incorporating tungsten material [1, 5]. Figure 5 illustrates the geometrical construction in which tungsten overlaps the copper thermocouples to securely hold the p-type and n-type thermoelectric legs.

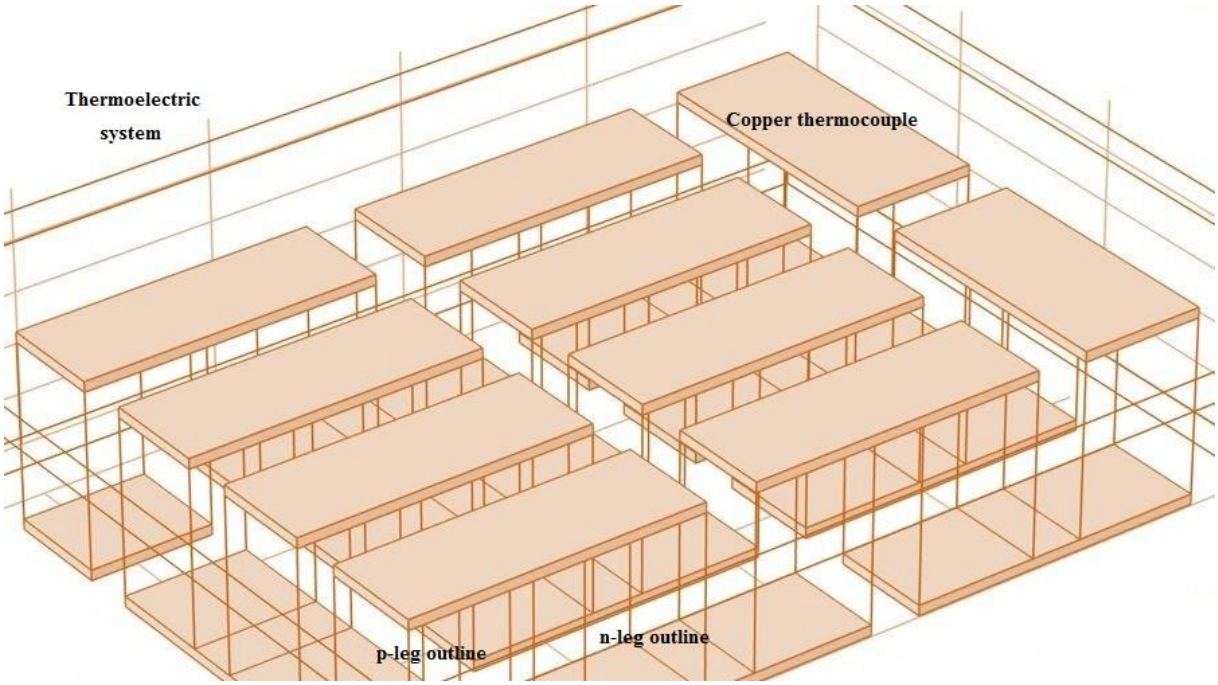

Figure 4. Architectural arrangement of copper thermocouple in thermoelectric system

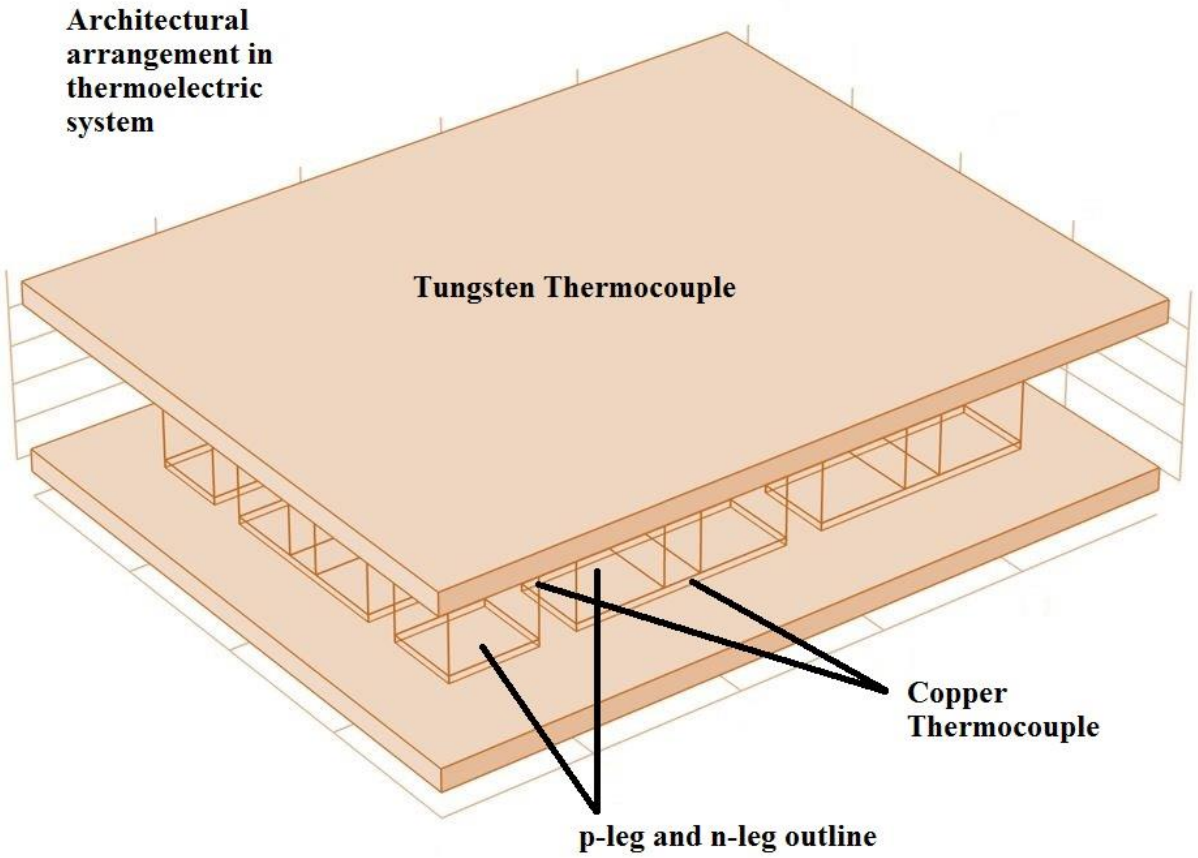

Figure 5. Architectural arrangement of tungsten-copper thermocouple in thermoelectric system

3. Performance Results

The performance of the thermoelectric system is evaluated based on coefficient of performance (COP). The variation in temperature across the p-type and n-type thermoelectric legs significantly influences the power generation and efficiency of the system. As the temperature difference increases, the output voltage and power are enhanced due to improved charge carrier transport [9, 12, 13]. The multistage configuration further improves system performance by enabling effective heat utilization across successive stages. Simulations performed by using COMSOL Multiphysics demonstrate that the optimized geometrical architecture and material arrangement contribute to enhanced thermoelectric performance and overall system efficiency. The system achieves a maximum temperature difference of 73.543 K at an operating current of 3.8237 A and a corresponding voltage of 1.4546 V. The overall electrical resistance of the system is found to be 0.64131 Ω, while the maximum heat dissipation reaches 2.5673 W, indicating effective thermal transport within the multistage configuration.

In Table 2, coefficient of performance varies significantly with both input current and applied temperature difference (ΔT_0). For $\Delta T_0 = 20$ K, the maximum COP of 1.48574 is obtained at a current of 0.35 A, demonstrating efficient cooling performance at lower temperature differences. When the temperature difference increases to 40 K, the maximum COP decreases to 0.596527 at a current of 0.5 A. At a higher temperature difference of 60 K, the COP further reduces, reaching a maximum value of 0.245475 at 0.7 A. This declination of COP with respect to increasing temperature difference is attributed to increased irreversible losses and higher electrical input requirements [18]. The results indicate that the thermoelectric system performs optimally at lower temperature differences, while higher temperature gradients lead to reduced efficiency despite of increased heat transfer capability [3]. The multistage thermoelectric architecture enables a significant temperature lift, making the system suitable for applications requiring moderate cooling with controlled power input. In Table 2, the negative value appeared in the COP is depend on thermal variation in the n-type and p-type leg with respect to thermocouple. The holes and carrier charges recombination is taken place in thermoelectric system.

Table 2. Current and COP for different temperature

Current	COP of T=20K	COP of T=40K	COP of T=60K
0.1	-0.742322	-5.85487	-8.4393
0.15	1.1343	-2.252	-4.4689
0.2	1.5665	-0.755615	-2.3594
0.25	1.664	-0.165694	-1.3727
0.3	1.56657	0.216559	-0.8629
0.31	1.49	0.21559	-0.8529
0.5	1.15541	0.596527	-0.05315
0.7	0.85204	0.44663	0.245475
0.9	0.55536	0.366021	0.13114

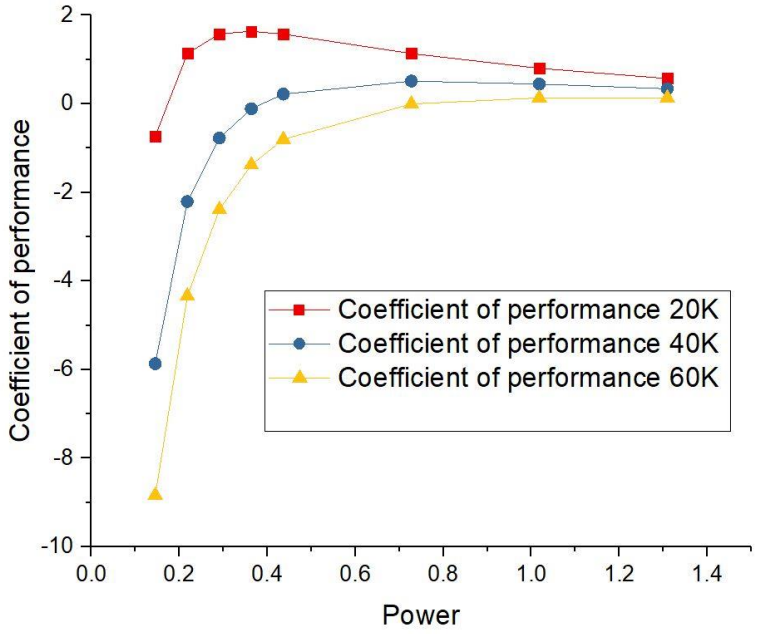

Figure 6. Power vs. COP of thermoelectric system

Electrical input power is supplied to the thermoelectric system during cooling operation. Figure 6 illustrates the variation of the coefficient of performance for temperature differences of 20 K, 40 K, and 60 K. The efficiency of the system is evaluated based on the geometrical construction of the copper–tungsten thermocouples integrated with Bi_2Te_3 p-type and Bi_2Te_3 n-type thermoelectric legs in thermoelectric system.

4. Conclusion

A comprehensive geometrical architectural framework for a multistage thermoelectric system has been successfully developed and analyzed by using COMSOL Multiphysics. The basic building blocks consisting of Bi_2Te_3 p-type and n-type thermoelectric legs integrated with copper and tungsten thermocouples were modeled in a three-dimensional configuration. The multistage arrangement enabled effective thermal utilization across successive segments for improvement of the overall system performance. It indicates that the geometrical construction plays a critical role in determining the coefficient of performance and temperature lift of the thermoelectric system. The proposed architecture achieved a maximum temperature difference about 73.543 K, with optimal COP values observed at lower temperature differences. As the temperature gradient is increased, the COP is decreased due to higher irreversible losses and increased electrical input requirements, which is consistent with thermoelectric operating principles. The integration of copper and tungsten thermocouples provided mechanical stability and effective electrical connectivity between the thermoelectric legs. The results confirm that multistage geometrical design and optimized thermocouple architecture significantly influence thermoelectric system efficiency. The developed framework offers a flexible and scalable approach for designing advanced thermoelectric cooling and waste heat recovery systems. Future works

may focus on experimental validation, material segmentation across stages, and further optimization of geometrical parameters to enhance performance under higher temperature gradients.

Declarations

Funding/Financial Disclosure The authors have no received any financial support for the research, authorship, or publication of this study.

Ethics Committee Approval and Permissions The work does not require ethics committee approval and any private permission.

Conflict of Interests The authors stated that there is no conflict of interest in this article.

References

[1] S. Ferreira Teixeira and A. M. Pereira, "Geometrical optimization of a thermoelectric device: Numerical simulations," *Energy Convers. Manage.*, vol. 169, pp. 217–227, 2018, doi: 10.1016/j.enconman.2018.05.030

[2] U. S. Ganesamoorthy, "Generalized Programming Idea for Making the Thermoelectric Device Using MATLAB Software for Cu2Bi2Te3 and Cu2Sb2Te3" *Int. J. Eng. Appl. Sci.*, vol. 15, no. 2, pp. 52–59, 2023, doi: 10.24107/ijeas.1261278.

[3] R. S. Kondaguli and P. V. Malaji, "Geometry design and performance evaluation of thermoelectric generator," *Eur. Phys. J. Spec. Top.*, vol. 231, no. 8, pp. 1587–1597, 2022, doi: 10.1140/epjs/s11734-022-00492-y.

[4] G. Li, S. Shittu, X. Ma, and X. Zhao, "Comparative analysis of thermoelectric elements optimum geometry between photovoltaic-thermoelectric and solar thermoelectric," *Energy*, vol. 171, pp. 599–610, 2019, doi: 10.1016/j.energy.2019.01.057.

[5] H. Li, S. E. Yang, and J. S. Son, "Computational methods for designing geometry-engineered thermoelectric devices," *J. Materiomics*, p. 101144, 2025, doi: 10.1016/j.jmat.2025.101144.

[6] H. C. Luo and L. S. Cheng, "Numerical study on optimizing the geometry of segmented asymmetrical thermoelectric generator," in *IOP Conf. Ser.: Earth Environ. Sci.*, vol. 701, no. 1, p. 012022, 2021, doi: 10.1088/1755-1315/701/1/012022.

[7] G. U. Sankar, G. Moorthy, and C. T. Ramasamy, "A review on recent opportunities in MATLAB software based modelling for thermoelectric applications," *Int. J. Energy Appl. Technol.*, vol. 8, no. 2, pp. 70–79, 2021, doi: 10.31593/ijeat.882470.

[8] G. U. Sankar, R. Yuvakkumar, G. Ravi, G. RajKumar, and C. G. Moorthy, "Preparation of CuO1-x-Mnx (x= 0.03, 0.05, 0.07) and MATLAB modelling for sustainable energy harvesting applications," *J. Phys.: Conf. Ser.*, vol. 1850, no. 1, p. 012025, 2021, doi: 10.1088/1742-6596/1850/1/012025.

[9] G. Udhaya Sankar, "Sustainable Energy Materials," in *Artificial Intelligence for Renewable Energy and Climate Change*, pp. 117–136, 2022, doi: 10.1002/9781119771524.ch5.

[10] G. Udhaya Sankar, C. Ganesa Moorthy, and G. J. E. S. RajKumar, "Synthesizing graphene from waste mosquito repellent graphite rod by using electrochemical exfoliation for battery/supercapacitor applications," *Energy Sources, Part A Recovery Util. Environ. Eff.*, vol. 40, no. 10, pp. 1209–1214, 2018, doi: 10.1080/15567036.2018.1476609.

[11] G. Udhaya Sankar, C. Ganesa Moorthy, and G. RajKumar, "Smart storage systems for electric vehicles–a review," *Smart Sci.*, vol. 7, no. 1, pp. 1–15, 2019, doi: 10.1080/23080477.2018.1531612.

[12] G. Udhaya Sankar, C. Ganesa Moorthy, and C. T. Ramasamy, “Mathematical Analysis on Power Generation—Part I,” in *Artificial Intelligence for Renewable Energy and Climate Change*, pp. 53–86, 2022, doi: 10.1002/9781119771524.ch3.

[13] G. Udhaya Sankar, C. Ganesa Moorthy, and C. T. Ramasamy, “Mathematical Analysis on Power Generation—Part II,” in *Artificial Intelligence for Renewable Energy and Climate Change*, pp. 87–115, 2022, doi: 10.1002/9781119771524.ch4.

[14] Y. Wu, J. Yang, Chen, S., and L. Zuo, “Thermo-element geometry optimization for high thermoelectric efficiency,” *Energy*, vol. 147, pp. 672–680, 2018, doi: 10.1016/j.energy.2018.01.104.

[15] G. U. Sankar and C. G. Moorthy, “Investigation on Thermoelectric Device Performance by modeling and simulations,” *J. Energy Trends*, vol. 2, no. 2, pp. 40–48, 2026.

[16] G. U. Sankar and C. G. Moorthy, “Optimization of materials for thermoelectric leg model device,” *World Sci. News*, vol. 211, pp. 190–199, 2026.

[17] G. U. Sankar and C. G. Moorthy, *The Book of Physics Formula*, 2025.

[18] G. U. Sankar and C. G. Moorthy, “Analysis of P-Type Bi_2Te_3 Thermoelectric Cooler Device Performance Using Embedded model,” *Selcuk Univ. J. Eng. Sci.*, vol. 24, no. 3, pp. 58–63, 2025, doi: 10.63673/sujes.693.

Sinop University
Positive Science International
e-ISSN: 3108-3862

Positive Science International, 2(1), 12-26
Research Article, Year: 2026
DOI: 10.71340/psi.1893297

Design and Analysis of Detachable Bolt Head (Zinc-Cap) From Zinc-Aluminum Series Alloys

Oğuz Gürkan GÜDER[1*], Sait Ozan YILMAZ[2], Sertaç EROL[3]

[1*]*Şa-Ra Energy Construction, Trade and Industry Inc., Design Engineer e-mail: oguzguder@sara.com.tr*
[2]*Şa-Ra Energy Construction, Trade and Industry Inc., Mold Design Leader, e-mail: ozanyilmaz@sara.com.tr*
[3]*Şa-Ra Energy Construction, Trade and Industry Inc., Design Manager, e-mail: sertacerol@sara.com.tr*

Article Info

Research article
Received: *03.03.2026*
Accepted: *21.05.2026*
Published: *30.06.2026*
Corresponding Author*:O. Gürkan GÜDER*
oguzguder@sara.com.tr
0009-0008-2581-8710

Keywords

Separable Bolt Head
Torque-Limiting Design
Mechanical Safety

Abstract

Bolted connections are essential components used in many engineering applications, particularly in power transmission lines where structures are subjected to severe vibrations and low-frequency oscillatory motions. These dynamic effects can lead to collisions of conductor bundles, mechanical wear, and reduced system stability. Therefore, separator dampers are installed to maintain conductor spacing and reduce vibration. However, for them to function correctly, their clamps must be tightened with precise torque values. Insufficient tightening can lead to clamp slippage, while overtightening can damage the conductor wires at aluminum-aluminum interfaces. To overcome this challenge, a torque-limiting, detachable bolt head called Zinc-Cap has been specially designed. The product consists of two sections connected by a deliberately tapered neck region. The upper section transmits torque during assembly, while the lower section grips the bolt head with a tight-fitting geometry. When the applied torque reaches a predetermined limit of 45 N.m, the shear zone breaks in a controlled manner, and the upper section separates from the lower section. This mechanism prevents overtightening and ensures the bolt remains consistently fixed at the correct torque value, regardless of the operator's skill.

ZA Serisinden Ayrılabilir Cıvata Başlığı (Zinc-Cap) Tasarımı ve Analizi

Makale Bilgisi

Araştırma makalesi
Başvuru: *03.03.2026*
Kabul: *21.05.2026*
Yayın: *30.06.2026*
Sorumlu Yazar*:
O. Gürkan GÜDER
oguzguder@sara.com.tr
0009-0008-2581-8710

Anahtar Kelimeler

Ayrılabilir Cıvata Başlığı,
Tork Sınırlayıcı Tasarım,
Kontrollü Kırılma, Mekanik Güvenlik.

Özet

Cıvatalı bağlantılar, özellikle yapıların şiddetli titreşimlere ve düşük frekanslı salınım hareketlerine maruz kaldığı enerji iletim hatlarında, birçok mühendislik uygulamasında kullanılan temel bileşenlerdir. Bu dinamik etkiler, iletken demetlerinin çarpışmasına, mekanik aşınmaya ve sistem kararlılığının azalmasına yol açabilir. Bu nedenle, iletken aralığını korumak ve titreşimi azaltmak için ayırıcı sönümleyiciler takılır. Ancak, doğru şekilde çalışabilmeleri için kelepçelerinin hassas tork değerleriyle sıkılması gerekir. Yetersiz sıkma kelepçe kaymasına yol açabilirken, aşırı sıkma alüminyum-alüminyum arayüzlerinde iletken tellerine zarar verebilir. Bu zorluğun üstesinden gelmek için, Çinko-Şapka (Zinc-Cap) adı verilen tork sınırlayıcı ayrılabilir bir cıvata başlığı özel olarak tasarlanmıştır. Ürünün kasıtlı olarak inceltilmiş bir boyun bölgesiyle birbirine bağlanan iki bölümünden oluşmaktadır. Üst bölüm montaj sırasında torku aktarırken, alt bölüm cıvata başlığını sıkı bir geçme geometrisiyle kavrar. Uygulanan tork önceden belirlenmiş 45 N.m sınırına ulaştığında, kesme bölgesi kontrollü bir şekilde kırılır ve üst kısım alt kısımdan ayrılır. Bu mekanizma, daha fazla sıkmayı önler ve cıvatanın, operatörün becerisinden bağımsız olarak, doğru tork değerine sürekli olarak sabitlenmesini sağlar.

To cite this article:
Güder O. G., Yılmaz S.O., and Erol S. (2026). Design and Analysis of Detachable Bolt Head (Zinc-Cap) From Zinc-Aluminum Series Alloys, Positive Science International, 2(1), 12-26, https://doi.org/10.71340/psi.1893297

1. Introduction

Bolted fasteners are widely utilized across engineering applications and are preferred as a fundamental joining method in numerous sectors, including electrical power transmission lines, structural steel configurations, and the automotive industry [1]. The widespread implementation of these connections renders the insurance of long-term durability and reliable operational performance a critical prerequisite [2].

Power transmission lines operate continuously under dynamic loads induced by environmental factors. In these systems, low-frequency, high-amplitude oscillations (galloping) represent a major technical challenge [3]. Such vibrations and oscillatory movements can cause the conductors within multi-bundle transmission lines to approach one another and collide [4]. To prevent this occurrence, spacer dampers are strategically positioned between the bundle conductors (Figure 1) [5].

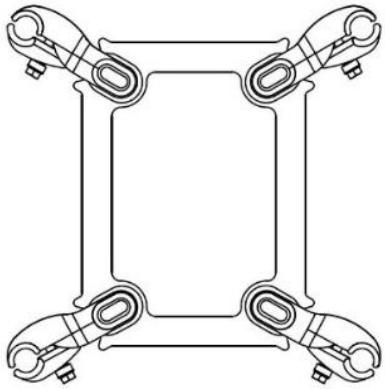

Figure 1. Two-dimensional view of a spacer damper

The spacer damper is a critical line component utilized to maintain a constant distance between bundle conductors in power transmission lines and to mitigate system-level vibrations [6]. To provide low density and corrosion resistance, the framework of this equipment is typically manufactured from aluminum alloys, whereas the elements responsible for vibration damping are fabricated from elastomer-based materials resilient to outdoor environmental conditions [7]. Concurrently, stainless or galvanized steel materials are preferred for the connection and clamp components due to high strength requirements [8].

Spacer dampers prolong the mechanical lifespan of conductors, preserve line stability, and prevent wear-induced damage by mitigating various vibration modalities, including Aeolian vibration, galloping, and sub-span oscillation [9]. Furthermore, they enhance system reliability by maintaining the integrity of the bundle structure under external environmental factors such as ice accumulation and wind loading [10].

The installation of spacer dampers requires strict precision to correctly adjust the inter-conductor spacing and to effectively achieve vibration-damping performance; therefore, it must be executed in accordance with relevant standards (Figure 2) [11]. During assembly, the clamps must be

tightened to a specific torque value, which is specified by the manufacturer to prevent the clamp from slipping along the conductor [12]. The proper selection of the installation torque is a critical parameter; insufficient tightening can lead to clamp displacement, whereas excessive tightening can cause permanent deformation in the conductor strands [13]. Particularly in connections involving aluminum-to-aluminum contact, undesirable phenomena such as structural deformation of the conductor and damage to the wire cores may arise. To avert these issues, regulating the applied installation torque is considered a vital engineering necessity [14].

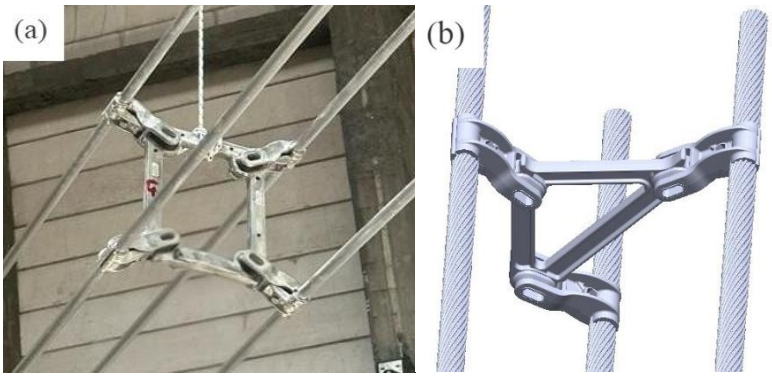

Figure 2. Four-bundle spacer damper (a), three-bundle spacer damper (b)

To eliminate operator-dependent variability during installation and to achieve a standardized tightening value across all components, a detachable bolt head (Zinc-Cap) has been developed (Figure 3). This component is designed as a two-part safety element with torque-limiting capabilities, manufactured from a zamac alloy. The upper section serves as the driving interface where torque is applied via a wrench, while the lower section features a tight-fit geometry that securely engages the hexagonal bolt head. These two segments are interconnected by a thin-walled, intentionally weakened fracture zone. The geometry and wall thickness of this cross-section constitute the most critical design parameters governing the shear failure torque of the system.

When the applied torque reaches the 45 N.m threshold during assembly, a localized stress concentration occurs within this zone. Upon exceeding the ultimate strength limit of the zamac material, a controlled fracture takes place. Following structural separation, the upper part detaches to interrupt further torque transmission, mechanically preventing the bolt from being tightened to higher torque values.

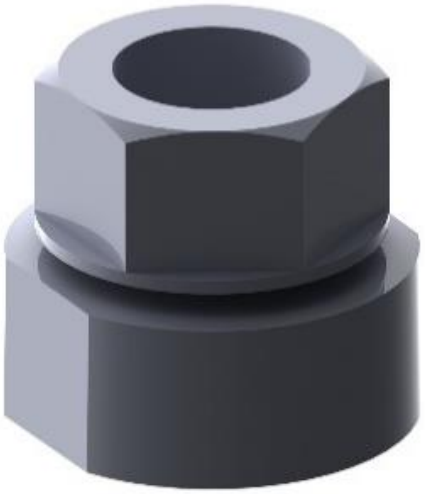

Figure 3. Solid model view of the adjustable bolt head

The performance of the detachable bolt head is not solely dictated by its geometric configuration but is directly linked to the material composition and production methodology. The high fluidity and castability of zamac alloys permit the manufacturing of thin-walled fracture zones with precise dimensional tolerances, which ensures consistent torque behavior across mass production lots [15]. The post-manufacturing surface finish enhances the structural reliability of the tight fit between the upper and lower sections, while the dimensional precision within the fracture zone ensures the reproducibility of the targeted 45 N.m torque limit. These characteristics render the detachable bolt head an effective, durable, and economical solution for mass production workflows, maintenance-free assembly lines, and engineering systems requiring rigorous torque control.

With this controlled fracture mechanism, the lower section remains fixed on the bolt head post-failure, while the upper section detaches from the system, completing its function. This structural configuration prevents the discarded fragments from scattering into the working environment and provides a visual verification that the joint has reached its target torque. The operating principle of the design relies on the synergetic optimization of the predictable mechanical properties of the zamac material and the precisely calculated geometry of the fracture cross-section [16].

This methodology minimizes part-to-part variation in fracture characteristics during production, thereby enhancing performance consistency and establishing a reliable torque-limiting mechanism for assembly operations [17]. Furthermore, the system protects both the bolt and the clamping components by mitigating the risk of over-tightening damage, standardizes installation quality, and provides an efficient solution for applications where mechanical safety is paramount.

2. Experimental Studies

2.1. Design Process

The design of the detachable bolt head was developed using a systematic engineering approach aimed at establishing a safety mechanism for torque limitation while ensuring high reproducibility in industrial assembly applications (Figure 4). The design sequence commenced with the definitions of application-specific requirements. In this context, a comprehensive set of design criteria was established, accounting for the target fracture torque (45 N.m), standard bolt dimensions, assembly constraints, environmental conditions, and preferred manufacturing methods.

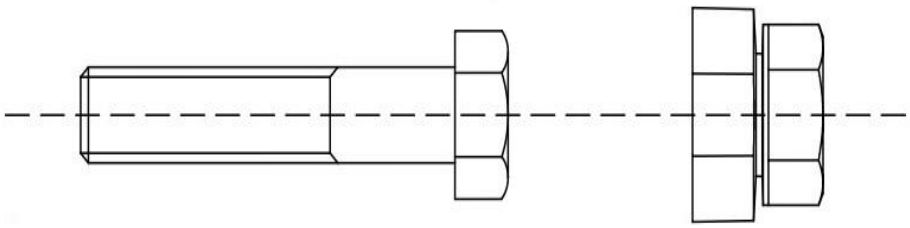

Figure 4. Assembly view of the adjustable bolt head

Based on these criteria, the functional architecture of the product was structured around two primary zones: an upper section shaped as a wrench hex interface for torque application, and a lower section that grips the bolt head to secure the connection. The geometric features of both components were optimized to provide adequate structural rigidity for torque transmission while maintaining dimensional accuracy during manufacturing.

The most critical stage of the design process involved the characterization of the thin-walled fracture zone situated between the upper and lower sections (Figure 5). Correctly configuring this region required iterative engineering studies to guarantee a controlled and repeatable fracture performance at the 45 N.m torque threshold. Consequently, optimization loops were conducted on the cross-sectional thickness, fracture perimeter length, transition radii, and potential stress concentration areas.

Finite element analysis (FEA), performed to simulate the mechanical behavior of the zamac material, mapped the stress and strain distributions, thereby identifying the location, intensity, and progression of the fracture. The simulations were directed to ensure that energy dissipates predictably through the thin-walled section, preventing sudden load releases from inducing structural damage to the bolt or the host assembly.

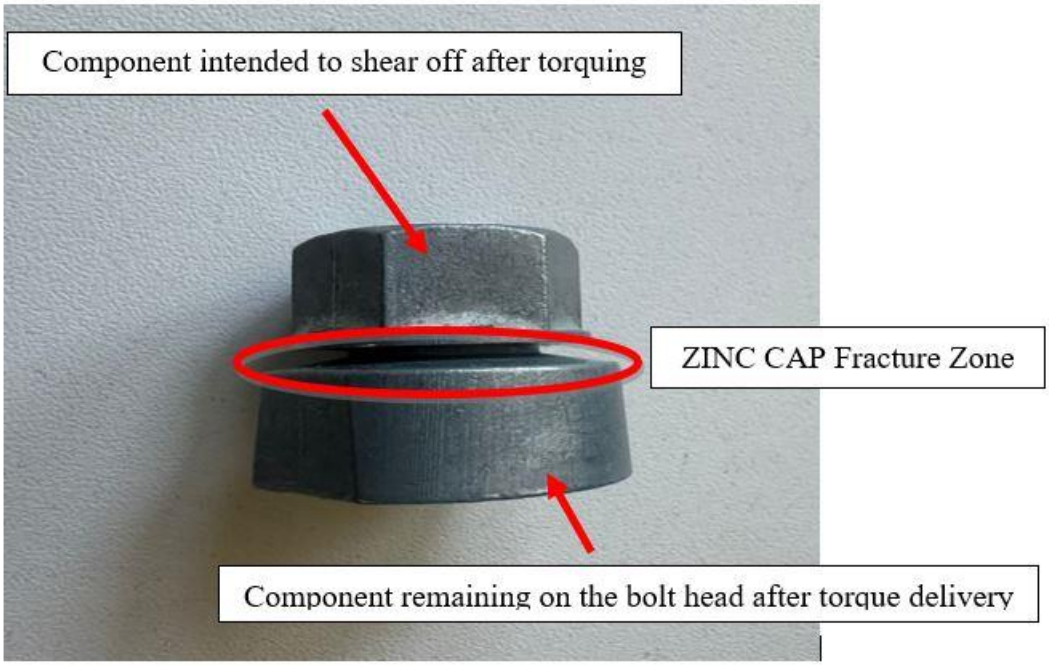

Figure 5. Functional sections of the adjustable bolt head

During the material selection phase, zamac alloy was chosen based on its die-casting precision and predictable fracture behavior (Table 1). This alloy facilitates the high-reproducibility manufacturing of the thin-walled fracture zone, ensuring a consistent torque limit across all production units (Table 2).

Table 1. Mechanical properties of Zamac 5

Mechanical properties of Zamac 5		
	Value	**Unit**
Density	6.6 - 6.8	g/cm³
Modulus of Elasticity	83	GPa
Yield Strength	200 - 250	Mpa
Ultimate Tensile Strength	300 - 330	Mpa
Hardness	90 - 120	HB

Table 2. Chemical composition of Zamac 5

Chemical composition of Zamac 5	
Element	Content (%)
Zinc (Zn)	95 - 96
Aluminum (Al)	3.5 - 4.3
Copper (Cu)	0.75 - 1.25
Magnesium (Mg)	0.03 - 0.06

Following the casting process, prototype testing was conducted to observe the actual behavior of the design under real torque loads. Laboratory measurements were cross-referenced with numerical

model results, and necessary design revisions were implemented. Consequently, the design was optimized through both analytical engineering calculations and experimental validation, establishing the detachable bolt head as a reliable, cost-effective torque-limiting product suitable for industrial environments.

2.2. Theoretical Calculation of the Fracture Zone

Geometrical and material properties of the component is given in Table 3.

Table 3. Geometrical and material properties of the component

Parameter	Value
Inner Diameter (d_i)	12.8 mm
Outer Diameter (d_o)	14.89 mm
Target Torque (T)	45 N·m = 45 000 N·mm
Material	Zamac 5
Yield Strength	~240 MPa
Shear Yield Strength	$\tau_\gamma \approx 0.6 \cdot \sigma_\gamma \approx 144$ MPa

Cross-sectional view of the detachable bolt head is given in Figure 6.

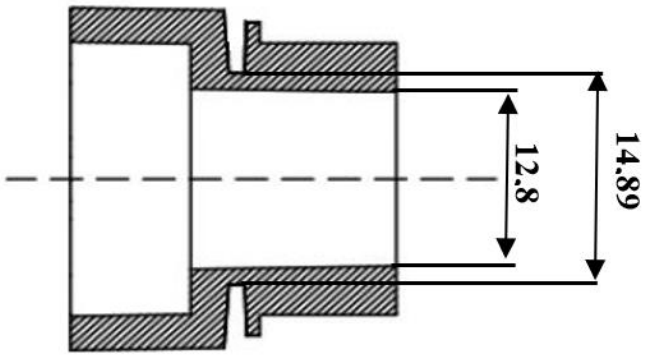

Figure 6. Cross-sectional view of the detachable bolt head

Polar Moment of Inertia (J)

Equation (1) and Equation (2) were used to calculate the polar moment of inertia (J) for the hollow circular cross-section:

$$J = \frac{\pi}{32}(do^4 - di^4) \quad (1)$$

$$do^4 = 14.89^2 = 49210\ mm^4$$

$$di^4 = 12.8^2 = 26844\ mm^4$$

$$J = \frac{\pi}{32}(49210 - 26844)$$

$$J = \frac{\pi}{32}(22366) = 2197\ mm^4 \quad (2)$$

Maximum Shear Stress (Tmax)

The maximum shear stress acting on the outer boundary of the shear zone was calculated using Equation (3), Equation (4), and Equation (5)

$$r0 = \frac{d0}{2} = 7.455\ mm \quad (3)$$

$$Tmax = \frac{T.r0}{J} \quad (4)$$

$$\mathrm{T}max = \frac{45000.7.455}{2197} \quad (5)$$

$$Tmax = 152.7\ \mathrm{MPa}$$

Calculated Shear Stress: 152.7 MPa

Typical Shear Yield Strength of Zamac 5: 144 MPa

Because the shear yield strength for the Zamac 5 alloy is rarely stated directly in literature, the Von Mises yield criterion ($\tau = 0.577\ \sigma_\gamma$), which is widely applied to ductile and semi-brittle metals, was adopted. Considering that literature reports yield strength values for this alloy within the range of 220–295 MPa, the shear yield strength was bounded between 130–170 MPa, and a nominal value of approximately 144 MPa was implemented for design calculations (Table 1) (ASM International, 2000; AZoM, 2023).

The torsional analysis executed within this study aimed to ensure that the designed Zamac 5 component exhibits a controlled yielding or fracture behavior under a torque of 45 N.m Accordingly, the cross-sectional dimensions were tailored to generate a stress level proximate to the material's shear limit. The analytical calculations indicated that the maximum shear stress of 152.7 MPa is highly close to the typical shear yield boundary of Zamac 5 (≈144 MPa). Consequently, the geometry was optimized to trigger the material's ultimate mechanical limit at the targeted loading threshold, validating the intended failure mechanism via an engineering-based analytical framework.

2.3 Computer-Aided Analysis of the Fracture Zone

In this study, the mechanical response of the connection element characterized by its thin transition cross-section and manufactured from Zamac 5 under an axial torque of 45 N.m was evaluated utilizing the ANSYS Static Structural finite element method (Figure 7). Within the numerical model, the lower mounting face was constrained in all degrees of freedom (fixed boundary condition), while a torsional moment of 45 N.m was applied along the central longitudinal axis of the upper region.

The stress distribution results indicate substantial stress concentrations localized at the thin-walled neck region where the primary body joins the upper section. Evaluation of the Von Mises equivalent stress field revealed a peak stress magnitude of approximately 339 MPa inside this critical zone.

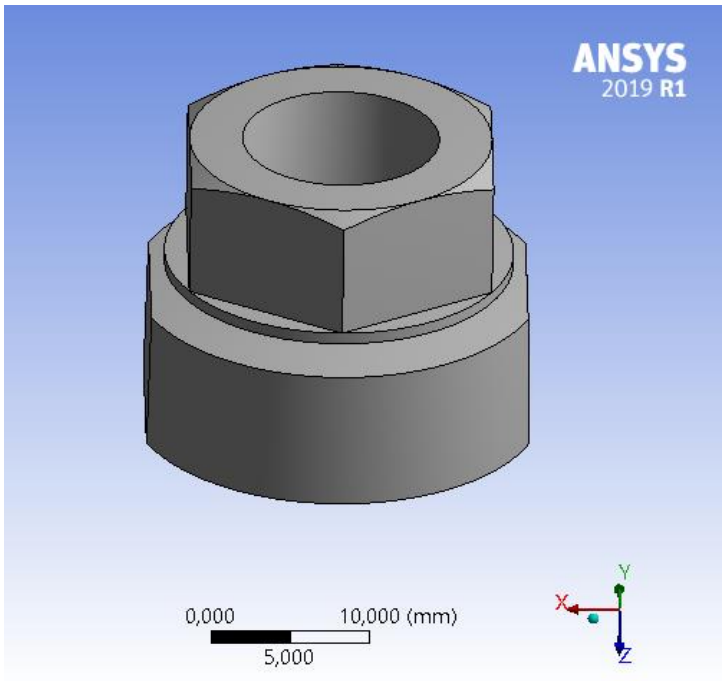

Figure 7. ANSYS finite element model of the adjustable bolt head

2.3.1 Mesh Modeling

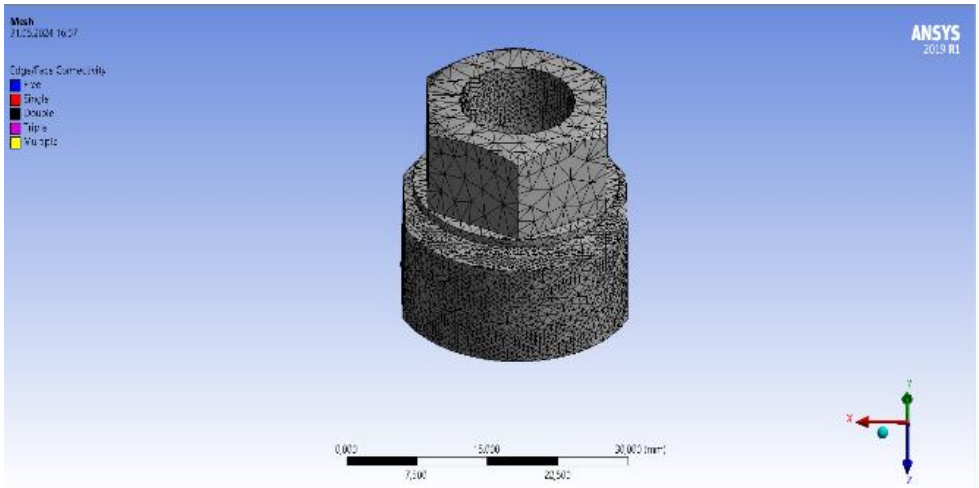

Figure 8. Mesh structure configuration

Table 4. Mesh statistics and configuration details

Mesh Properties	
Physics Preference	Mechanical
Element Order	Linear
Element Size	0.5 mm
Element Type	Tetrahedral
Number of Nodes	8030
Number of Elements	27826

To enhance the numerical accuracy of the finite element analysis, an optimized mesh topology was generated (Figure 8). Linear tetrahedral elements with a nominal size of 0.5 mm were prescribed for the discretization (Table 4). To capture high-gradient stress fields with precision, adaptive mesh refinement was enabled, dynamically increasing element density within regions susceptible to fracture. A fast-transition algorithm was applied to prevent abrupt volumetric variations between adjacent elements at geometric discontinuities.

The geometric fidelity of the model was verified by monitoring mesh quality metrics, including minimum edge length and average face area. Furthermore, the convergence criteria, error bounds, and smoothing parameters were tuned to ensure the physical validity of the stress and strain distributions, yielding a highly realistic simulation of the component behavior.

2.3.2 Boundary Conditions

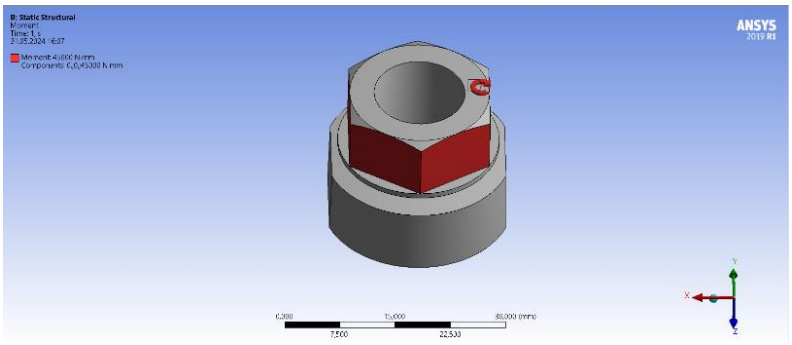

Figure 9. Application of torque to the numerical model

During the definition of boundary conditions, the mating interface located at the base of the bolt head was fixed, and a pure torsional moment was applied to the upper hexagonal manipulation zone to run the simulation (Figure 9). This boundary configuration replicated the physical testing apparatus and installation environment closely.

2.3.3 Material Specifications

Table 5. Mechanical constants of Zamac 5 utilized in FEA

Mechanical Property	Value (MPa) / Constant
Ultimate Compressive Strength	600 MPa
Compressive Yield Strength	250 MPa
Tensile Yield Strength	240 MPa
Ultimate Tensile Strength	330 MPa
Modulus of Elasticity	82.500 MPa
Poisson's Ratio	0.25

Prior scientific investigations conducted by Coşkun et al. indicate that ZA-5, ZA-12, ZA-14, ZA-22, and ZA-50 alloys are unsuitable for cold deformation processes. This is attributed to the dual-phase ($\alpha + \eta$) microstructural network inherent to Zamac alloys (such as Zn-4Al). The presence of the hexagonal close-packed (HCP) eta (η) phase restricts the global ductility of the material. The HCP structure possesses a layered configuration with limited active slip systems, which hinders dislocation

motion—the primary mechanism governing metallic plasticity. Because HCP metals cannot activate a sufficient number of independent slip systems during cold deformation, they exhibit a macroscopically brittle behavior [18].

For this reason, the brittle characteristic of the Zamac 5 alloy was deemed highly suitable for the functional requirements of this study. This mechanical property enables components manufactured via hot-chamber die casting to attain elevated dimensional accuracy with minimal geometric deviation in series production. Moreover, once the target torque threshold is achieved, the ultimate fracture resistance of this material aligns more effectively with the design limits than conventional ductile alternatives (Table 5).

2.3.4 Analysis Results

Given that the ultimate tensile strength of Zamac 5 is 330 MPa and its tensile yield strength is 240 MPa, the calculated maximum Von Mises stress (339 MPa) exceeds both the elastic limit and the ultimate tensile strength threshold of the material. This condition establishes that under the nominal installation load, the material transcends its elastic regime into significant plastic deformation, indicating a high probability of structural failure during subsequent loading phases.

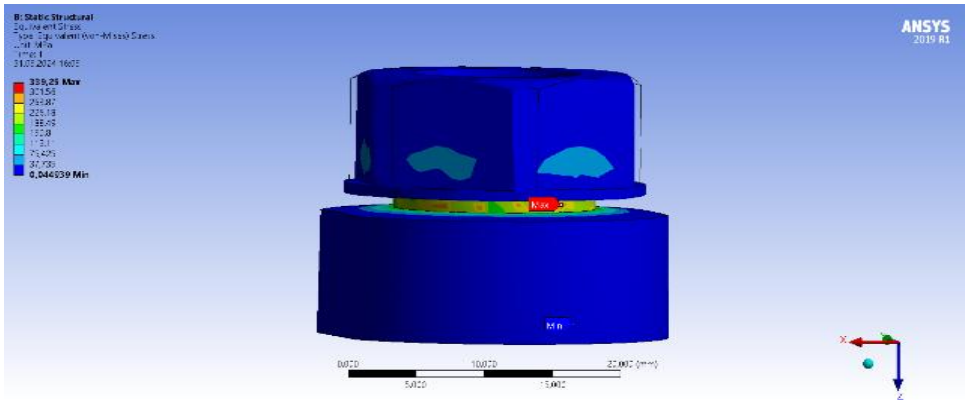

Figure 10. Von Mises equivalent stress contours of the adjustable bolt head

Although the maximum isolated shear stress was recorded at a modest 116 MPa (Figure 11), equivalent (Von Mises) stresses were utilized as the primary metric for failure prediction because the component is subjected to a multi-axial state of stress under external loading (Figure 10). Within this framework, the prediction of mechanical fracture at a torque of 45 N.m correlates with the numerical data. The thin-walled neck region acts as a structural weak point that cannot sustain the applied moment, thereby exceeding the safety envelope of the design and triggering failure at approximately 45 N.m.

Nevertheless, numerical simulations and analytical formulations do not independently constitute definitive evidence; they must be evaluated in conjunction with empirical data to form a holistic engineering conclusion.

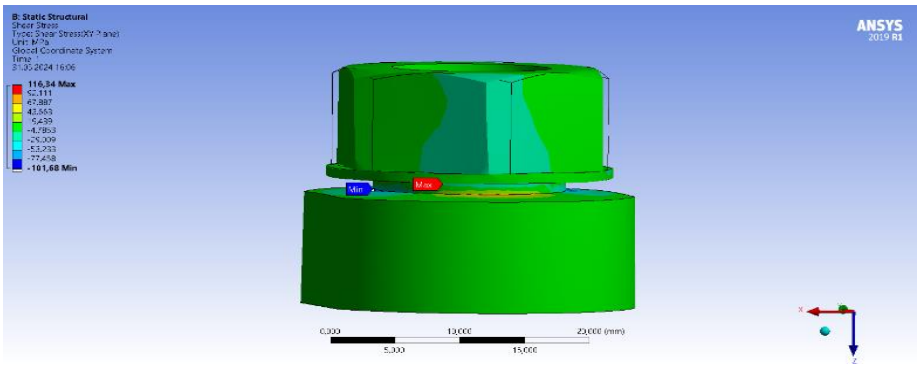

Figure 11. Shear stress contours of the adjustable bolt head

2.4 Experimental Testing

Upon concluding the analytical and numerical design phases, the components were fabricated from commercial-grade Zamac 5 via hot-chamber die casting for mass production validation (Figure 12). Post-production samples were assembled with matching structural elements to simulate final field conditions and subjected to destructive torque testing.

To ensure measurement accuracy and statistical reproducibility, a calibrated digital torque wrench was employed. According to design specifications, the component was required to undergo controlled fracture within a target tolerance band of 45 N.m ± 10%, corresponding to an acceptable operational range between 40.5 Nm and 49.5 Nm.

Figure 12. Adjustable bolt head samples post-die casting

Empirical testing demonstrated that all evaluated specimens underwent structural failure strictly within the prescribed tolerance band. This outcome indicates that the die-casting process successfully imparts the targeted mechanical properties to the component in a reproducible manner, confirming the failure behavior predicted by the finite element models. Consequently, it is scientifically validated that the requirement for a controlled detachment around 45 N.m is satisfied, exhibiting close correlation between numerical simulations and experimental verification.

The die-cast components were fitted onto the hexagonal portion of standard bolts and subjected to tightening tests using a digital torque evaluation apparatus (Figure 13). The experimental procedure

was applied to 10 distinct specimens, utilizing identical instrumentation and the same operator to eliminate external variables. The compiled data fell entirely within the specified safety limits, with no anomalous structural behavior observed (Table 6). Furthermore, the testing confirmed that the detachable cap successfully interfaces with the hexagonal bolt geometry and locks rigidly to prevent premature loosening prior to failure.

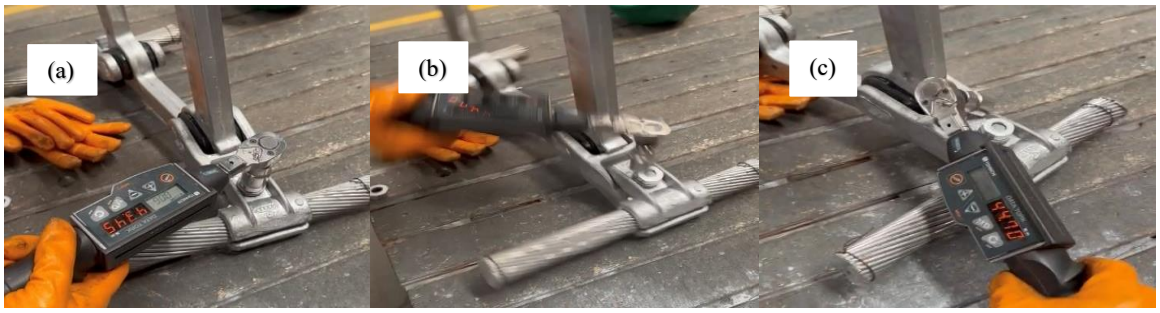

Figure 13. Torque testing sequence; (a) pre-fracture state, (b) moment of fracture, (c) post-fracture state

Table 6. Spacer damper reference torque test data

ZINC CAP TORQUE TEST										
Sample No	1	2	3	4	5	6	7	8	9	10
Torque Value (45 N.m ±%10)	42.75	44.2	46.3	44.7	45.9	43.5	47.3	44.1	46.8	43.3
Test Results	✓	✓	✓	✓	✓	✓	✓	✓	✓	✓

3. Results and Discussion

Within the scope of this investigation, the controlled fracture performance of a safety connection component manufactured from Zamac 5 was comprehensively evaluated at a target torque value of 45 N.m via analytical, numerical, and experimental methodologies. The primary objective of the design was to establish an intentional "controlled weak point" that fractures when the external load surpasses a critical threshold, thereby decoupling the mechanical drive to prevent over-loading and safeguard primary structural systems. Consequently, 45 N.m was mandated as the critical failure torque.

To achieve this objective, the elasto-plastic behavior of the material was initially evaluated using classical mechanics formulations. Analytical calculations incorporating the specific cross-sectional geometry, loading mode, and material strength values (330 MPa), (240 MPa) indicated that the thin transition zone would exceed its yield limit under a 45 N.m torsional load. This finding matches the design premise that stress concentration within the neck region triggers failure. This preliminary assessment, grounded in fundamental mechanical principles, provided a strong baseline indication of the component's failure profile.

Following the analytical work, an ANSYS Static Structural finite element analysis was executed to resolve the stress fields within the geometry. By fixing the lower boundary and applying a pure 45 N.m torsional moment about the central axis, a maximum Von Mises equivalent stress of 339 MPa was recorded at the neck. This value exceeds both the yield and tensile strength limits of Zamac 5, verifying that the component enters the plastic deformation regime and initiates fracture precisely within this zone under the target load. Moreover, the stress concentration confirms that the geometric reduction successfully acts as a localized stress amplifier. The numerical findings demonstrate an elevated degree of correlation with the initial analytical calculations.

To validate the theoretical and numerical models, physical specimens were produced via die casting and subjected to experimental torque testing inside an automated assembly setup. Quantitative measurements obtained via a digital torque wrench showed that all tested components fractured within the 45 N.m ± 10% envelope 40,5 – 49,5 N.m. The tight clustering of these failure points validates both the reproducibility of the manufacturing method and the structural reliability of the engineering design. These experiments prove that while analytical calculations and numerical simulations are essential predictive tools, their integration with empirical data yields a robust and definitive engineering conclusion.

From a holistic perspective, all three branches of this study analytical calculations, finite element modeling, and physical torque testing exhibit high convergence. The agreement of these independent methodologies regarding the failure envelope reinforces the scientific validity of the design and confirms that the component successfully achieves its protective safety function. This validation process demonstrates that the geometric configuration, material selection, and casting parameters are mutually optimized.

In terms of practical engineering applications, this research presents a reliable, repeatable methodology for designing torque-limiting fasteners. The developed Zinc-Cap minimizes operator-induced error during installation, ensuring a standardized tightening quality across field assemblies. Furthermore, by mechanically restricting excessive torque, it protects adjacent connection elements and conductor structures, increasing overall system safety. This design approach provides a practical, cost-effective solution for structural fastening problems, particularly in overhead power transmission lines where variable field conditions make standardized maintenance and installation paramount.

Declarations

Acknowledge: The authors express their gratitude to the Şa-Ra Enerji A.Ş. R&D Center for providing the necessary facilities, equipment, and technical support during the experimental testing phase of this study.

Conflict of Interest: The author declares that there is no conflict of interest regarding the publication of this paper.

Funding: This research received no specific grant from any funding agency in the public, commercial, or not-for-profit sectors.

References

[1] R. C. Juvinall and K. M. Marshek, *Fundamentals of Machine Component Design*. Wiley, 2017.

[2] J. H. Bickford, *An Introduction to the Design and Behavior of Bolted Joints*. CRC Press, 2007.

[3] R. Claren and G. Diana, "Galloping of Overhead Transmission Lines," *J. Wind Eng.*, 1996.

[4] C. B. Rawlins, *Transmission Line Reference Book*. EPRI, 2010.

[5] *Guide for Spacer Damper Applications on Overhead Lines*, IEEE Std 563-2022.

[6] "Spacer Dampers for Bundle Conductors," CIGRE Technical Brochure 799, 2020.

[7] M. Shariat et al., "Elastomer Materials for Vibration Damping," *Mater. Eng.*, 2021.

[8] G. E. Totten, *Handbook of Aluminum*. CRC Press, 2018.

[9] M. Irvine, "Dynamic Behavior of Conductors," *Electr. Power Syst. Res.*, 1990.

[10] O. Nigol and G. Clarke, "Wind and Ice Effects on Bundle Conductors," *IEEE Trans. Power Deliv.*, 1987.

[11] *Overhead Lines – Requirements and Tests for Spacer Dampers*, IEC 61284.

[12] *Fasteners—Mechanical Properties of Bolts*, ISO 898-1.

[13] B. Housari, "Overtightening Failures in Mechanical Connections," *Eng. Fail. Anal.*, 2018.

[14] R. Budynas and J. Nisbett, *Shigley's Mechanical Engineering Design*. McGraw-Hill, 2020.

[15] J. Campbell, *Complete Casting Handbook*. Elsevier, 2015.

[16] R. Hertzberg, *Deformation and Fracture Mechanics of Engineering Materials*. Wiley, 2012.

[17] M. Çelik, "Tekrarlanabilir Tork Sistemleri Üzerine Deneysel Bir Çalışma," *Endüstriyel Tasarım ve Mekatronik Dergisi*, 2023.

[18] G. Coşkun, "Proceedings of the 5th International Symposium on Characterization," in *Proc. ISC'25*, Cappadocia, Türkiye, 2025, p. 754.

Sinop University
Positive Science International
e-ISSN: 3108-3862

Positive Science International, 2(1), 27-42
Research Article, Year: 2026
DOI: 10.71340/psi.1866014

Microbial Analysis, Physicochemical Content and Insect Vectors Associated with Selected Dumpsites in Ijebu-Ode, Nigeria

Adewole SEBIOMO[1*]

[1*] *Department of Biological Sciences, Tai Solarin Federal University of Education Ijagun, Nigeria*

Article Info

Research article
Received: *18.01.2026*
Accepted: *10.03.2026*
Published: *30.06.2026*
Corresponding Author*: *Adewole SEBIOMO*
sebiomoadewole6@gmail.com
0000-0002-3930-0022
Keywords

Insect
Bacteria
Fungi
Viabe counts

Abstract

This study analyzed the types of insect vectors in dumpsite locations and the microorganisms associated with the insect vectors and dumpsites. The heavy metal and physicochemical content of the soil samples were also determined. Bacteria and fungi were isolated from the soils, housefly and cockroaches collected from the dumpsites. Atomic absorption spectrophotometer was used to determine the mineral content of the soil samples. Bacterial and fungal counts were also determined using the Quebec colony counter. Dehydrogenase, phosphatase, catalase, urease and peroxidase activities were estimated. Of the ten bacterial species identified *Pseudomonas aeruginosa* had the highest frequency of 20.3% while *Streptococcal faecalis* had the least percentage frequency of 3.1%. Seven fungal genera were identified. They include; *Aspergillus niger*, *Trichoderma* spp., *Penicillium* spp. the enzyme activities in this work increased significantly ($P \leq 0.05$) after analysis of dumpsite soils. Peroxidase and catalase activities of dumpsite soils were higher compared to their control soil samples. The Na, Fe, Zn, Cu, Pd and Cd contents of the dump site soil samples were more than what was obtained in the control soil samples. However, the Ca, Mg, K contents of the control soil samples were significantly higher than those of the dump site soils. Fe had the highest value of 33.57±10.22 mg/kg compared to the other soil samples.

Nijerya'nın Ijebu-Ode Bölgesinde Seçilmiş Çöp Depolama Alanlarıyla İlişkili Mikrobiyal Analiz, Fizikokimyasal Bileşim ve Böcek Vektörleri

Makale Bilgisi

Araştırma makalesi
Başvuru: *18.01.2026*
Kabul: *10.03.2026*
Yayın: *30.06.2026*
Sorumlu Yazar*: *Adewole SEBIOMO*
sebiomoadewole6@gmail.com
0000-0002-3930-0022
Anahtar Kelimeler

Böcek
Bakteri
Mantar
Canlı sayımı

Özet

Bu çalışmada, çöp depolama alanlarında bulunan böcek vektörlerinin türleri ile bu böcek vektörleri ve depolama alanlarıyla ilişkili mikroorganizmalar incelenmiştir. Ayrıca, toprak örneklerinin ağır metal ve fiziko-kimyasal içerikleri de belirlenmiştir. Çöp depolama alanlarından toplanan toprak, ev sineği ve hamamböceği örneklerinden bakteri ve mantarlar izole edilmiştir. Toprak örneklerinin mineral içeriklerinin belirlenmesinde atomik absorpsiyon spektrofotometresi kullanılmıştır. Bakteri ve mantar sayımları ise Quebec koloni sayacı kullanılarak gerçekleştirilmiştir. Dehidrogenaz, fosfataz, katalaz, üreaz ve peroksidaz enzim aktiviteleri değerlendirilmiştir. Tanımlanan on bakteri türü arasında, %20,3'lük görülme sıklığı ile *Pseudomonas aeruginosa* en yüksek orana sahip olurken, %3,1'lik görülme sıklığı ile *Streptococcus faecalis* en düşük orana sahip olmuştur. Yedi mantar cinsi tanımlanmıştır. Bunlar arasında *Aspergillus niger*, *Trichoderma* spp. ve *Penicillium* spp. yer almaktadır. Çalışmada incelenen çöp depolama alanı topraklarında, analizler sonrasında enzim aktivitelerinde anlamlı düzeyde artış ($P \leq 0,05$) gözlenmiştir. Depolama alanı topraklarının peroksidaz ve katalaz aktiviteleri, kontrol toprak örneklerine kıyasla daha yüksek bulunmuştur. Çöp depolama alanı topraklarında belirlenen Na, Fe, Zn, Cu, Pb ve Cd içerikleri, kontrol topraklarında elde edilen değerlerden daha yüksek bulunmuştur. Buna karşın, kontrol topraklarının Ca, Mg ve K içerikleri, depolama alanı topraklarına göre anlamlı derecede daha yüksek olarak belirlenmiştir. İncelenen elementler arasında Fe, 33,57 ± 10,22 mg/kg değeri ile en yüksek konsantrasyona sahip olmuştur.

To cite this article:
Sebiomo, A. (2026). Microbial Analysis, Physicochemical Content and Insect Vectors Associated with Selected Dumpsites in Ijebu-Ode, Nigeria, Positive Science International, 2(1), 27-42, https://doi.org/10.71340/psi.1866014

1. Introduction

Wastes are usually disposed at selected locations or recycled for other uses. In times past, wastes have not shown any important environmental impact due to the recycling processes occuring in the soil. The rise in population of man and industries, resulted in the increased rate at which waste is generated resulting in significant environmental changes. Due to poor waste management technologies in many underdeveloped nations [1], environmental pollution, disease causing organisms, toxins, heavy metals, toxic gaseous emissions, and other dangerous pollutants have increased. These wastes are usually generated from agriculture, industries and other anthropogenic activities. The production of waste in Nigeria is more than two hundred and fifty thousand tons every year. It is produced more in the urban areas compared to the rural areas [2]. The quantity of wastes and dumpsites in Nigeria have increased drastically due to unprecedented rise in human population, construction, businesses and manufacturing industries [3]. When wastes accumulate, they negatively impact the quality of the soil in that environment. Unchecked rise in waste products affects the capacity of soils to naturally handle the waste. When pollution occurs soil microflora and soil fauna are impacted. Fluctuations in pH, temperature, electrical conductivity and microbial populations, are some of the factors which show the impact of pollutants in the environments [4].

Accumulation of waste can be attributed to the rise in population when people move from the rural areas to the cities. Waste dumpsites is a breeding ground for rodents, mosquitoes, flies and pathogenic microorganisms [5]. In most developing countries wastes are usually deposited on roads without proper care for waste disposal. Improper management of solid wastes results in land degradation, water pollution and air pollution. Proliferation of dump sites usually reduces the soil quality and which usually results in decrease of vegetation abundance. Important sources of heavy metals in dump sites are wastes from industries, ashes from incinerators, wastes from mines and dangerous substances from households such as dyes, paints, batteries, inks, etc. [6]. This causes adverse effects on human and animal health as well as the soil fertility and soil quality. Accumulation of wastes in dump site gives rise to exponential multiplication of bacteria and fungi which in turn degrades the substances that are biodegradable [5]. A lot of households in Nigeria rely on groundwater for their daily activities. Dumpsites can pollute groundwater by via a mixture of industrial wastes [7]. Biodegradable wastes in dump sites decays and then smells generating methane gas which, increases the greenhouse effect. Burning wastes is discouraged because plastic releases substances which are toxic and dangerous such

as dioxins. Biodegradable wate can acts as breeding grounds for disease transmitting insects and rodents, which transmits diseases such as cholera, diarrhoea, dysentery and typhoid fever.

Dumpsites are a common occurrence in Ijebu ode local Government of Ogun state, Nigeria. A lot of pathogenic microorganisms and insect vectors which spread these microbes are usually associated with these dumpsites. The wastes sometimes end up in soils useful for agriculture via erosion and then resulting in contamination of rivers and drinking water supplies. The dumpsites are of primary health concern because of the spread of pathogenic microorganisms. On the other hand, accumulation of wastes could result in increase in microbial load which enables the conversion of organic matter to inorganic matter which in turn supplies plant nutrients. Consequent upon accumulation of wastes in the dumpsites there is usually a resultant accumulation of minerals and heavy metals in soils after biodegradation of the wastes. Hence the aim of this study is to determine the microbial activities, physicochemical content, and insects associated with the dumpsite soils via the following objectives; (1) Isolation and identification of microorganisms associated with dumpsite soils, (2) Determination of the urease, phosphatase, dehydrogenase, peroxidase and catalase activities in dumpsite soils, (3) Analysis of the pH, electrical conductivity, organic carbon, nitrogen, phosphorus, calcium, magnesium, potassium, sodium, iron. zinc, copper, lead and cadmium content of dumpsite soil samples, (4) Identification of insects associated with the dumpsites, (5) Isolation of the microorganisms associated with these insects.

2. Materials and Methods

2.1. Sampling Location

This work was conducted in Ijebu ode local government, Ogun state, Nigeria. The research location occurred between longitude 3.180 E and latitude 6.470 N in Nigeria. The area is a rain forest region that has both dry and wet seasons. The annual rainfall is always high with values in the range of 1575-2340

2.2. Sample Collection

A total of 30 soil samples was collected from ten different dump sites in Ijebu Ode local government Ogun state. Soil samples, approximately 100 g each, were collected from the selected dumpsites using soil auger at a depth of 5 cm, thus ensuring minimal disturbance to the soil structure. Control soil samples were collected from distance located at least 150 meters away from the dump site to assess baseline conditions. The collected soil samples were carefully transferred into black polythene bags, labelled accordingly, and transported to Biochemistry laboratory, Institute of Agricultural Research and Training, Moor Plantation, Apata, Ibadan, Oyo state, for further analysis. All samples were analyzed within 24 h of collection and stored in a cool, dry place prior to examination. A composite sampling technique was employed to ensure representative samples from each site. Four locations were chosen in a grid format to facilitate comprehensive analysis.

In addition to the samples from the dump sites.

2.3. Collection of Insects

- Sticky traps: The cockroaches were trapped using sticky traps. It was made with plywood. The plywood is 60 cm long, 40 cm wide and two cm thick. The plywood was coated on the surface with grease and placed at the dumpsite so that the insects were caught when they approached it.
- Water traps: They were designed with plastic buckets (5 litres in volume). The buckets were filled with water and detergents were introduced into the water to reduce surface tension and enhance wetting of the insects [8].
- **Sweep net:** They were used for catching the houseflies in this study. They were made using mosquito nets. Metal rods were used to form the rim and a wooden handle was added. Twenty sweeps were carried out at a dumpsite between 8.00am and l0.00am in the morning for a better catch.
- **Hand picking:** Cockroaches were also handpicked. Samples were collected in the morning between 8-10 am.

2.4. Microbial Enumeration and Identification

Twenty-eight grams of Nutrient Agar powder was weighed on the Mettler balance and dispensed into 1000ml of distilled water contained in the conical flask. It was dissolved and then distributed into macCartney bottles before it was sterilized in autoclave set at 121°C for 15 minutes. 55g of macConkey Agar was weighed on analytical meter balance and dissolved in 1000ml of distilled water in clean and dry conical flasks. It was dissolved and then distributed into macCartney bottles before it was sterilized in autoclave set at 121°C for 15 minutes. Thirty-nine grams of Potato Dextrose Agar was weighed on analytical meter balance and dissolved in 1000ml of distilled water in a clean and dry conical flask. It was dissolved and then distributed into macCartney bottles before it was sterilized in autoclave set at 121°C for 15 minutes. Nine milliliters of distilled water were pipetted into a clean test-tube and were covered with cotton wool and foil then placed in autoclave at 121°C for 15 minutes to produce sterile water. After this 1 gram each of soil sample was weighed into test-tube containing 9 ml of sterile distilled water and serially dilute them into 5 test-tube.

Pour plate method was used to dispense the inoculum into the culture plates. The plates were then allowed to cool and set. Each sample were duplicated and the plates were incubated at 37°c for 24-48 hrs. Nutrient Agar and MacConkey agar while the Potato Dextrose Agar was incubated at 28°c-30°c. All the plates were incubated invertedly. After bacteria and fungi emerged from plates, they were sub-cultured continuously until pure cultures were achieved. Quebec colony counter was then used to count bacteria and fungi in culture plates containing 15-150 colonies per plate and then the colony forming units per gram (cfu/g) was calculated. Pure culture of bacteria isolated was identified on the basis of their morphological and biochemical characteristic. The organisms were subsequently characterized according to the taxonomic scheme of Buchanon and Gibbon, (1974) while fungi were identified base on morphological and cultural characteristics.

2.5. Phosphatase Activity

Two grams of soil sample was extracted with 20ml sodium carbonate buffer at pH 6.0. The suspension obtained was centrifuged at 5000 rpm in a high speed Gerber centrifuge (Gallenkamp model) at 5ºC for 30 min. The supernatant obtained at the end of 30 min centrifugation was decanted into 30 ml centrifuge stoppered bottle and stored in a deep freezer at -20ºC prior to analysis. One ml of enzyme extract of sample was pipetted into 50 ml test tube. five ml of disodium-p-nitrophenol phosphate was added, mixed thoroughly by shaking to obtain a homogenous solution and left to stay for 5 minutes in order to yield the yellowish colouration. A standard solution of phosphatase enzyme was prepared from stock phosphatase solution and treated similarly like the sample above. The absorbance of the yellowish colour solution and standard solution was measured as change in 60s (1 min) at wavelength of 475nm. One unit of phosphatase activity was estimated as the quantity of enzyme which catalysed 0.01 absorbance change in one min at wavelength of 475 nm.

$$\text{Phenol } (\mu g\ g^{-1}\ dwt\ h^{-1}) = \frac{C \times 100}{dwt \times t \times 10}$$

C = phenol concentration (µg phenol ml^{-1}) filtrate

dwt = dry weight of 1g moist soil

t = the incubation time hours,

100 is the total volume of the soil suspension in millitres

10 is the weight of the soil used in the test.

2.6. Soil Urease Activity

Urease activity was determined using the method of and Teicher [9]. After incubation of soil with urea and citrate buffer addition urease activity was measured using a colorimeter. Prior to incubation, toluene was added.

2.7. Dehydrogenase Activity

The method of Kumar *et al.* [10] was adopted in this study to determine the dehydrogenase activity of soil samples. Five grams of the soil samples treated with Dimethylammonium acetate and Nicosulfuron+Atrazine and non-treated soil samples were dispensed into 250 mL conical flask. TTC-glucose solution (1 mL) and Tris buffer (2.5 mL) solution were added to the herbicide-treated soil samples. One mL of distilled water was then added into the control flasks. The pH was adjusted to 7 using 1.0 N HCl and the flasks were swirled gently to mix the contents. The mixtures were incubated at 30 °C for 24 hours. After incubation, the soil samples were treated with methanol and transferred into a funnel and then sieved with Whatman No 42 filter paper placed on 100 mL graduated cylinder. Additional amounts of methanol were passed through the soil until 50 mL of methanol, containing the formazan, was collected in the graduated cylinder. The red methanolic solutions of the formazan were determined using a UV/Vis Spectrophotometer.

2.8. Peroxidase Activity

Peroxidase activity was measured using the method of Burns [11]. Peroxidase activity in soil samples was measured using the spectrophotometer. Pyrogallol was then used as substrate. A suspension containing 0.1 g of fresh soil to which 25 ml of 50 mMsodium acetate buffer at pH 5 was then homogenized for 1 minute. The activity of the peroxidase enzyme was measured by adding 1 mL of soil suspension to two hundred and fifty microlitre of substrate solution. The substrate and buffer, soil suspension and buffer were then prepared. The buffer was used as blank. Five microlitre of 0.3% hydrogen peroxide was dispensed to each sample and the controls. The prepared samples were incubated at 20°C (in the dark) for four hours. Peroxidase activity was then determined in the spectrophotometer at a wavelength of 460 nm. The activity of enzyme peroxidase was then calculated and values were expressed in μmol/g soil/h [15].

2.9. Catalase Activity

Catalase activity was determined using the method described by Vijayakumar *et al.* [17]. Residual H_2O_2 was titrated with $KMnO_4$ [16]. One gram of soil sample was dispensed into 5 mL distilled water with 1 mL of 3% hydrogen peroxide solution. The resultant solution was then shaken vigorously and five mililitres of 1.5 mol/L H_2SO_4 was latter added. The resulting solution was then filtered. Titration was done using 0.05 mol/L $KMnO_4$. One enzyme unit was calculated as the amount of enzyme that catalysed the consumption of 1 μmol of H_2O_2 per g soil per hour [17].

2.10. Mineral, pH and Electrical Conductivity Analysis

The method described by Blakmore *et al.* [18] was used to determine the mineral contents of the vegetables. Concentrations of minerals (Na, K, Ca, Fe and Zn) in the samples were estimated using the atomic absorption spectrophotometer. Sample extract and standard solutions were introduced into the atomic absorption spectrophotometer. The concentrations of the minerals were then calculated. Cadmium (Cd), Lead (Pb), Hexavalent Chromium (Cr^{+6}) and Mercury (Hg) were analyzed, in air dried soil samples obtained from polluted auto mechanic workshop sites after the soils have been homogenized, by using the atomic absorption spectrophotometer. The pH and electrical conductivity (EC) of the samples were determined using pre-calibrated pH and conductivity meter.

2.11. Statistical Analysis

The version 20 of the statistical package for social sciences (SPSS) software was used to analyze data from the microbial count, soil nutrient content, soil microbial respiration and soil biomass carbon. Duncan's tests and the One-Way ANOVA were used to test statistical differences between the various treatment groups. Continuous data are presented as Mean ± standard deviation and were considered statistically significant when the p-values were less than 0.05.

3. Results

Table 1 shows the dominance of *Clostridium* spp. (Bacteria), *Enterobacter melanogenicum* (Bacteria), *Fusarium* spp. and *Aspergillus* spp. (Fungi) in majority of the soil samples analyzed.

Table 1. Bacteria and fungi obtained from dumpsite soil samples

Soil Samples	Bacteria	Fungi
CONTROL	*Streptococcus aureus*	*Fusarium* spp.,
SOFAARI1	S. *pyogenes, Enterobacter melanogenicum, Bacillus* spp., *Clostridium* spp.	*Aspergillus* spp., *Fusarium acacia*
SOFAARI2	*Psedomonas aeruginosa, Escherichia coli, Staphylococcus aureus, Bacillus* spp., *Acinetobacter* spp.	*Fusarium poliferatum, Mucor mucedo*
SOFAAR13	*Salmonella typhi, S. saprophyticuss, P. putida*	*Mucor racemosus, Penicillum chrysogenum*
SO1TONR1	*E. melanogenicum, S. pyogenes, E. coli, Acinetobacter* spp.	*Penicillum* spp., *Aspergillus nodulans*
SOITONRI2	*Clostridium spp., Bacillus* spp*., S. aureus, Klebsiella pneumonia*	*Saccharomyces* spp., *Fusarium oxysporum*
SOITONRI3	*Salmonella* spp*., P. aeruginosa, S. aureus, Bacillus* spp.	*Mucor* spp., *Penicillum chrysogenum, Aspergillus* spp.
SOSABOO1	*Clostridum* spp., *S. pyogenes, E. melanogenicum, Salmonella typhi*	*ochraceus, Penicillum* spp*., Fusarium acacia*
SOSABOO2	*P. aeruginosa, E. coli, S. aureus*	*Saccharomyces* spp., *Mucor mucedo*
SOSABOO3	*Bacillus* spp., *S. saprophyticus, K. pneumonia*	*nodulans, Fusarium proliferatum*
	S. pyogenes, Clostridium spp., *E. coli*	*Fusarium oxysporum, Saccharomyces* spp., *Aspergillus* spp.

The following are soil samples obtained from Faari; SOFAARI1, SOFAARI2, SOFAARI3, Itorin; SO1TONR1, SO1TONR2, SO1TONR3 and Sabo; SOSABOO1, SOSABOO2, SOSABOO3

Contained in Table 2 are ten genera of bacteria namely *Acinetobacter* spp., *Pseudomonas aeruginosa*, *Escherichia coli* and *Streptococcus faecalis.* Of the ten bacterial species identified *P. aeruginosa* was consistently isolated in all the samples collected. It recorded a percentage frequency of 21.3% while *S. faecalis* were the least with a percentage frequency of 4.1%.

Table 2. Bacterial Isolates obtained from Dumpsites and their Percentage Occurrence in Soil Samples

Bacterial isolates	Percentage occurrence
Acinetobacter spp.	18.6
S. faecalis	4.1

P. aeruginosa	21.3
Serratia spp.	8.9
B. subtilis	15.8
S. aureus	8.6
Escherichia coli	3.9

The results presented in Table 3 shows the fungi isolated from the dumpsites. Seven fungal genera were identified these includes *Aspergillus niger*, *Trichoderma viride Penicillium notatum*., *A. niger* recorded the highest occurrence with a percentage frequency of 25.44% while *Fusarium* spp. recorded the percentage frequency of 9.10%.

Table 3. Fungal isolates from dumpsites and their percentage occurrence in soil samples

Fungi isolates	% Frequency of occurrence
A. niger	25.44
T. viride	10.70
P. notatum	17.90
F. oxysporum	10.10
Mucor mucorales	22.0
Saccharomyces cerevisiae	13.00
Rhizopus stolonifer	12.20

Table 4 shows the enzymatic activities of the soil samples. Dehydrogenase and urease (21.97± 11.00 mg/g and 98.90± 15.93 mg/g) had the highest activities at Faari and Itorin respectively. In this study enzyme activities increased significantly compared to the control.

Table 4. Enzyme Activities of Soil Samples

Parameters	Control	Faari	Itorin	Sabo
Urease (mg/g)	8.50±0.00	70.77±29.88	98.90±15.93	59.73±7.0
Acid Phosphatase	1.70±00	1.95±0.05	0.98±0.42	0.98±0.12
Alk. Phosphatase	1.60±0,00	0.70±0.30	1.03±0.57	0.76±0.42
Dehydrogenase (mg/g)	5.20±0,00	21.97±11.00	12.93±0.96	11.50±5.0
Peroxidase(µmol/h/g)	0.38±0.04	5.09±0.60	1.30±0.69	1.40±0.20
Catalase(µmol/h/g)	<0.01	0.03±0.01	0.0±0.01	0.04±0.01

Presented in Table 5 are the microbial counts of the soil obtain from the dumpsite. There was significant difference ($p \leq 0.05$) in the actinomycetes counts. The highest count of $8.94 \pm 0.88 \times 10^2$ was obtain at the Itonri dumpsite. The lowest actinomycetes count of $6.17 \pm 0.58 \times 10^2$ cfu/g was obtained from the control soil samples. The actinomycetes counts ranged from 6.17 ± 0.58 to $3.85 \pm 1.45 \times 10^2$ cfu/g. There was significant difference ($p \leq 0.05$) in the bacteria count. The highest count value of $3.85 \pm 1.45\ 10^2$ cfu/g was obtained at the Faari dumpsites. The lowest fungi count of $2.95 \pm 0.58 \times 10^2$

cfu/g was obtained from the control soil sample the fungi counts ranged from 2.95 ± 0.58 to 3.85 ± 1.45 $\times 10^2$ cfu/g. There were significant differences ($p \leq 0.05$) in the bacterial counts. The highest count value of 5.19 ± 1.15 $\times 10^2$ cfu/g was obtained at the Sabo dumpsite. The lowest bacteria count of 3.11 ± 0.57$\times 10^2$ cfu/g was obtained from the control soil sample. The bacteria counts ranged from 3.11 ± 0.57 $\times 10^2$ cfu/g to 5.19 ± 1.15 $\times 10^2$ cfu/g. The bacterial count value of 4.23 ± 0.88 $\times 10^2$ cfu/g obtained at Itonri dumpsite was significantly higher than what was obtained at the other sampling points. The lowest coliform count of 2.16 ± 0.57 $\times 10^2$ cfu/g was recorded in the control soil sample. The coliform count ranged from 2.16 ± 0.57 to 4.22 ± 0.88 $\times 10^2$ cfu/g.

Table 5. Microbial Counts of Dumpsite Soils

	TAC (cfu/g $\times 10^2$)	TFC (cfu/g $\times 10^2$)	TBC (cfu/g $\times 10^2$)	TCC (cfu/g $\times 10^2$)
CONTROL	6.17±0.58^{a}	2.95±0.58^{a}	3.11±0.570^{j}	2.16±0.57^{a}
SOFAARI1	7.63±1.55^{d}	3.74±1.87^{e}	3.39±0.88^{a}	3.23±1.15^{c}
SOFAARI2	8.47±1.45^{j}	3.55±1.15^{c}	3.89±1.15^{e}	3.72±1.45^{g}
SOFAAR13	7.71±1.15^{e}	3.85±1.45^{d}	3.49±1.45^{c}	3.37±1.15^{d}
SO1TONR1	7.20±1.15^{d}	3.85±1.45^{e}	3.17±1.45^{a}	3.05±1.45^{b}
SOITONRI2	8.94±0.88^{k}	3.76±1.15^{e}	5.34±1.45^{i}	4.23±0.88^{k}
SOITONRI3	7.81±1.45^{f}	3.52±0.88^{cd}	3.56±1.73^{d}	3.49±1.45^{f}
SOSABOO1	7.55±1.45^{c}	3.35±1.76^{c}	3.37±1.45^{b}	3.49±1.45^{f}
SOSABOO2	8.31±1.45^{i}	3.16±1.45^{b}	5.19±1.15^{h}	4.11±1.15^{j}
SOSABOO3	8.15±1.45^{g}	3.06±1.15^{ab}	5.04±1.15^{f}	3.86±1.45^{h}

The following are soil samples obtained from Faari; SOFAARI1, SOFAARI2, SOFAARI3, Itorin; SO1TONR1, SO1TONR2, SO1TONR3 and Sabo; SOSABOO1, SOSABOO2, SOSABOO3. TAC= Total Actinomycetes count, TFC= Total Fungal Count, TBC= Total Bacterial Count, TCC= Total Coliform Count

The result presented in Table 6 shows the physical and chemical characteristics of the soil samples obtained from the dumpsites. The soils of the dumpsites and control all recorded acidic pH values. The highest pH value of 6.33 recorded at Itorin, Sabo and control dumpsites while the lowest pH value of 5.80 was obtained at Faari. Nitrogen content was highest in the samples from the dumpsites (0.24 ± 0.00%) compared to the control. However, the lowest Total Nitrogen concentration (0.10 ± 0.00%) was obtained in the control. Phosphorus showed similar trends comparable to that of the soil nitrogen. It recorded the highest concentration (7.94 ± 3.96%) at Faari. The lowest concentration of 3.30 ± 0.00% was recorded in the control soil samples. Samples from the various sampling point had high amount of sand compared to clay and slit. Samples obtained from Sabo recorded the highest amount of sand (85.93 ± 4.11%), while soil samples obtained from Sabo recorded the lowest amount of sand (74.20±4.127%). There were significant differences ($p \leq 0.05$) in the mineral and heavy metal content of soil samples. The Na, Fe, Zn, Cu, Pd and Cd contents of the dump site soil samples were significantly higher than their control soil samples. However the Ca, Mg, K contents of the control soil samples were significantly higher than those of the dump site soils. Fe had the highest value of 33.57 ± 10.22 mg/kg compared to the other soil samples.

Table 6. Physicochemical Properties of Dumpsite Soils

Parameters	Control	Faari	Itorin	Sabo
Ph	7.27±0.25	5.80±0.18	6.33±0.25	7.23±0.35
Electrical conductivity (µS/cm)	23.38±0.7	69.30±5.23	87.10±5.74	39.70±3.12
Total organic carbon (%)	0.73±0.00	4.82±0.87	2.80±1.32	2.14±0.25
Nitrogen (%)	0.16±0.00	1.33±0.16	0.24±0.00	0.13±0.6
Phosphorus (%)	3.33±0.00	7.94±3.96	6.67±3.49	4.70±3.75
Sand (%)	88.62±0.0	74.20±4.12	75.80±11.54	88.93±4.67
Silt (%)	7.00±0.00	9.30±1.90	10.03±4.24	4.97±1.37
Clay(%)	4.00±0.00	19.53±4.55	16.20±7.36	9.807±3.31
Ca (meq/100g)	2.80±0.00	1.55±0.64	1.10±0.70	0.90±0.51
Mg (meq/100g)	2.90±0.00	0.77±0.13	0.57±0.22	0.47±0.21
K (meq/100g)	0.90±0.00	0.45±0.12	0.29±0±15	0.33±0.06
Na (meq/100g)	0.40±0.00	0.35±0.16	0.33±0.10	0.23±0.06
Fe (mg/kg)	0.90±0.00	33.57±10.23	17.14±3.08	10.63±6.45
Zn (mg/kg)	0.12±0.00	2.53±1.03	0.85±0.24	0.70±0.36
Cu (mg/kg)	0.02±0.00	0.70±0.27	0.29±0.23	0.30±0.00
Pb (mg/kg)	<0.01	0.87±0.14	0.14±0.06	0.05±0.01
Cd (mg/kg)	ND	0.06±0.05	0.03±0.01	ND

In Table 7, the cockroaches obtained from Sabo recorded the highest (TVC), (TBC), (TYC) and (TMC). ($6.35 \pm 0.01\times10^3$ cfu/g, $4.45 \pm 0.01\times10^3$cfu/g, $3.05 \pm 0.02\times10^3$, $1.40 \pm 0.01\times10^3$ cfu/g, $1.54 \pm 0.01\times10^3$ cfu/gestectively). The TVC($5.88 \pm 0.04\times10^3$ cfu/g) of cockroaches obtained from Faari recorded the lowest counts of $5.88 \pm 0.04 \times10^3$ cfu/g compared to Itonri ($6.25 \pm 0.01\times10^3$ cfu/g) and Sabo ($6.35 \pm 0.01\times10^3$ cfu/g). The TBC of cockroaches obtained from IJELE also recorded the lowest TBC value of $3.20 \pm 0.05\times10^3$ cfu/g. There was significant ($p \leq 0.05$) difference in the TVC, TBC, TFC and TMC value.

Table 7. Viable Counts of Microorganisms Obtained from Cockroaches

LOCATION	TVC×10^3 cfu/g	TBC×10^3 cfu/g	TFC×10^3 cfu/g	TYC×10^3 cfu/g	TMC×10^3 cfu/g
ITONRI	6.25 ± 0.01^b	3.55 ± 0.01^b	2.88 ± 0.44^a	1.32 ± 0.01^b	1.43 ± 0.01^b
FAARI	5.88 ± 0.04^a	3.20 ± 0.05^a	2.77 ± 0.47^a	1.20 ± 0.03^a	1.34 ± 0.23^a
SABO	6.35 ± 0.01^c	4.45 ± 0.01^c	3.05 ± 0.02^b	1.40 ± 0.01^c	1.54 ± 0.01^c

This results in Table 8 indicates the presence of bacteria in the cockroach samples obtained from the selected dumpsites. Pathogenic bacteria such as *S. aureus, S. typhi, K. pneumonia, E. coli* and *S. pyogenes* were identified. The other isolated bacteria include *Puesdomonas aureginosa, Actinetobacter calcoceticus, Puesdomonas maltophilia, Serratia marcescens, Bacillius* spp., *Yersinia enterocolitica, Salmonella typhi, Clostridium* spp., *Listeria monocytogenes* and *Enterobacter melangenicum.*

Table 8. The Bacteria Isolated from Cockroaches

FAARI	ITONRI	SABO
P. aeruginosa	*S. marcescens*	*S. pyogenes*
Streptococcus spp.	*Bacillius* spp.	*E. coli*
K. pneumonia	*Y. enterocolitica*	*P. maltophilia*
A. calcoceticus	*S. typhi*	*L. monocytogenes*
P. maltophilia	*Clostridium* spp.	*E. melangenicum*
E. coli	*S. pyogenes*	
	P aeruginosa	

In Table 9, *Aspergillus* spp. and *Fusarium* spp. which include *Aspergillus niger, Aspergillus terreus, Aspergillus cereus, Aspergillus fumigatus, Fusarium compactium, Fusarium oxysporium* were commonly isolated from all the cockroach samples collected from the dumpsites.

Table 9. The Fungi Isolated from Cockroaches

FAARI	ITONRI	SABO
A. niger	*F. compactium*	*A. terreus*
S. cerevisae	*P. oxalicum*	*A. flavus*
A. cereus	*A. niger*	*F. oxysporium*
A. tamari	*A. terreus*	*A. fumigatus*
P. oxalicum	*S. cerevisae*	*S. cerevisae*
Fusarium oxyporium		*Trichoderma haraium*

The bacteria isolated from housefly collected from dumpsites (Table 10) include; *Salmonella typhi, Escherichia coli, Actinetobacter calcoceticus, Yersinia enterocolitica, Staphylococcus aureus, Proteus* spp.*, Kieblesiella pneumonia, Puesdomonas maltophilia, Serratia marcescens, Streptococcus pyogenes, Pseudomonas aeruginosa, Enterobacter melangenicum, Listeria monocytogenes, Clostridium* spp. *and Bacillius* spp.

Table10. The Bacteria Isolated from Houseflies Obtained from Different Dumpsites.

FAARI	ITORIN	SABO
S. typhi	*E. coli*	*A. calcoceticus*
Y. enterocolitica	*S. aureus*	*S. aureus*
Proteus spp.	*K. pneumonia*	*P. maltophilia*
S. marcescens	*A. calcoceticus*	*S. pyogenes*
P. aeruginosa	*P. maltophilia*	*E. coli*
S. pyogenes		*E. melangenicum*
		L. monocytogenes,
		Clostridium spp.
		Bacillius spp.

In Table 11, *Aspergillus niger, Trichoderma harzianum, Aspergillus fumigates, Fusarium compacticum, Penicillum oxalicum, Aspergillus tarrus, Saccharomyces cerevisae, Fusarium oxysporium and Aspergillus cereus* were obtained from housefly obtained from all the dumpsites examined in this study.

Table 11. The Fungi Isolated from Houseflies Obtained from Different Dumpsites.

FAARI	ITONRIN	SABO
F. compacticum,	*A. niger*	*T. harzianum*
P. oxalicum	*P. oxalicum*	*A. fumigatus*
A. terreus	*A. cereus*	*A. niger*
S. cerevisae	*A. tamari*	*F. oxysporium*
A. niger	*F. oxysporium*	

4. Discussion

The dumpsites that were analysed in this study were found to be at varying decomposing stages. This shows the poor sanitary condition in the locality. The most important challenge to environmental health arose from accumulated municipal solid waste and human excreta. The analysis of waste dumpsite in Ijebu Ode showed that coliform organisms mainly of human origin were prevalent in the soil samples. In this study pathogenic bacteria (i.e. *Salmonella typhi*) and fungi (i.e. *Aspergillus fumigatus*) were isolated from the cockroaches and houseflies examined in this study. This indicates a possible spread of diseases if the insects are not eliminating and the dumpsites cleared of refuse.

The bacterial activity in the dumpsites could be due to putrefaction and increased decomposition of organic matter in the vicinity of the dumpsites. *Escherichia coli*, an indicator of fecal pollution, was obtained in dumpsite soils analysed in this study. *Enterobacter melanogenicum* was also found to be predominant in all dumpsite soil samples. Ekundayo *et al.* [28] reported that seven (7) different species of bacteria were isolated (*Clostridium* sp., *Bacillus* spp., *Staphylococcus aureus*, *Klebsiella pneumoniae*, *Pseudomonas aeruginosa*, *Escherichia coli* and *Salmonella* spp.) in their study. The work of Nireti *et al*. [29] also correlated with the results in this study. They isolated *Escherichia coli*, *Klebsiella* spp., *Pseudomonas* spp., *Staphylococcus aureus* and *Streptococcus* spp., and fungi isolates *Aspergillus niger*, *Mucor* spp., *Penicilluim* spp. and *Saccharomyces* spp. *Fusarium oxysporum* and *Penicillum* spp. were in all dumpsite soils compared to the control. The work of Obueh *et al*. [19] reported the isolation microorganisms that were also isolated in this study. In their study, seven bacterial species were isolated. *F. oxysporum* has been shown to be pathogenic in plants. However, *Penicillum* spp., have antibacterial activities. *Streptococcus pyogenes* and *S. aureus* were also predominant in the dumpsite soils. These two have been implicated in bacterial infection in man (blood). *P. aeruginosa* and *Acinetobacter* spp. had the highest frequency of occurrence of 20.3% and 15.6% respectively. The following fungal genera were the most predominantly. Isolated: *A. niger*, *Tricoderma* spp., *Penicillum* spp., *Aspergillus nige*r

had the highest percentage frequency of 22.4%. *A. niger* have been shown to produce Aflatoxins in the substrates where the grow. The urease, Acid phosphatase, Alkaline phosphatase, dehydrogenase, peroxidase and catalase activities were more prominent in dumpisite soils compared to the control. The increased microbial activities in the dumpsite soil is indicative of rise in biodegradation rates. Obueh *et al.* [19] also reported that the pH values in their work ranged from 5.26 ± 0.03 to 6.87 ± 0.04. Permissible pH limit recommended by WHO [20] is 6.5-8.5. Ibiam *et al*. [21] stated that the excessive amounts of phosphate in the well water, will result in the multiplication of algae and latter result in slime production, which negatively impacts the quality of water.

Several physicochemical characteristics of the waste dump soil were assessed in this study. Ohaeri *et al*. [30] reported that the dumpsites analysed in their study yielded the following pH results: Umuchima (7.11), Eziobodo dumpsite (7.08), and Girls Hostel (6.97). Ohaeri *et al*. [30] further stated that a number of variables pertaining to the breakdown and interaction of waste products with the environment may be responsible for the higher pH values found in the dumpsite soils. Paper goods, yard debris, and food scraps are examples of organic waste items that break down over time. In this study there were no significant differences ($P \geq 0.05$) in the pH values obtained in this study.

The organic carbon, total nitrogen and available phosphorus levels were significantly higher than control. The accumulation of organic carbon in the dumpsites might be as a result of excessive combustion that is carried out constantly on the dump sites. Ohaeri *et al*. [30] corroborated the results obtained in this study. They discorvered that the organic carbon values in dump site soils were higher than control values. In this study the Na, Fe, Zn, Cu, Pd and Cd contents of the dump site soil samples were significantly higher than their control soil samples. The increased values of heavy metals occurred as a result of the excessive accumulation of waste materials that contained heavy metals. The Ca, Mg, K contents of the control soil samples were significantly higher than those of the dump site soils. Bhalla *et al*. [22] opined that heavy metals pollution of boreholes and wells occurs as a result of infiltration of the landfill leachate through the water.

Taofeek *et al*. [31] reported that in all the investigated soils, concentrations of Fe were the highest followed by Mn. This is similar to the results obtained in this study where Fe had the highest value. Odu *et al.* [23], stated that water that contains high amounts of chromium will result in allergic dermatitis and cancer. It could also cause cancer in the human body [24]. Udofia *et al*. [25] reported lead poisoning could retard brain development and the ability to learn in children.

The bacteria and fungi isolated from houseflies and cockroaches obtained from the dumpsite soil samples are pathogenic and could spread from the insects to man and animals after contact with food or open wound. Samuel *et al.* [26] were able to isolate *Aspergillus flavus, A. niger, Penicillium* spp., and *Fusarium* spp. in their work. They also reported that the average temperature obtained from the dumpsite was 270C and the average pH obtained was 7.7. Abba *et al.* [8] reported that nine insect species were collected from refuse dumps studied. They further stated that the species of insect were

different in the refuse dumps analysed. *M. domestica, Anopheles* spp. and *P. americana* were collected and examined.

5. Conclusion

The viable counts of bacteria, fungi and actinomycetes were highest in dumpsite soils. The microbial activities were in the dumpsite soils were higher compared to the control showing higher degradation rates in the dumpsite soils. Pathogenic bacteria and fungi were consistently isolated from the insects and dumpsite soils. This however shows high possibility for the outbreak of bacterial or fungal infections in areas located close to the dumpsite soils.

Acknowledgements

Funding/Financial Disclosure The authors have no received any financial support for the research, authorship, or publication of this study.

Ethics Committee Approval and Permissions The work does not require ethics committee approval and any private permission.

Conflict of Interests The authors stated that there is no conflict of interest in this article.

References

[1] A. L. Al-Khatib, M. Maria, A. Salam, A. Zahra, H. Q. Shahen, and D. Kassinos, "Solid waste characterization, quantification, and management practices in developing countries," *J. Environ. Manage.*, vol. 91, no. 5, pp. 1131–1138, 2010, doi: 10.1016/j.jenvman.2010.01.003.

[2] F. I. Okoronkwo and G. C. Okpokwasili, "Open refuse dumpsites: effect on soil and underground water in Port Harcourt metropolis," *Int. J. Dev. Res.*, vol. 8, no. 4, pp. 19765–19775, 2018.

[3] B. O. Ojiego, S. A. Abdullahi, I. M. K. Gadzama, P. I. Bolorunduro, and A. Arowosebge, "Characterization of solid waste at Gosa dumpsite, Federal Capital Territory, Abuja," *Int. J. Sci. Res. Rev.*, vol. 8, no. 3, pp. 414–419, 2019.

[4] B. Onwuka and B. Mang, "Effects of soil temperature on some soil properties and plant growth," *Adv. Plants Agric. Res.*, vol. 8, no. 1, pp. 34–37, 2018, doi: 10.15406/apar.2018.08.00288.

[5] M. S. Ayilara, O. S. Olanrewaju, O. O. Babalola, and O. Odeyan, "Waste Management through Composting: Challenges and Potentials," *Sustainability*, vol. 12, no. 11, p. 4456, 2020, doi: 10.3390/su12114456.

[6] P. Alam and K. Ahmade, "Impact of Solid Waste on Health and The Environment," *Int. J. Sustain. Dev. Green Econ.*, vol. 2, pp. 165–168, 2013.

[7] A. T. Adewole, "Waste management towards sustainable development in Nigeria: A case study of Lagos State," *Int. NGO J.*, vol. 4, no. 4, pp. 173–179, 2009.

[8] E. Abba, M. Amina, Y. R. Lamogo, A. Jemimah, and K. P. Yoriyo, "Survey of Insect Vectors in Some Selected Dumpsites in Gombe Metropolis, Nigeria, Western Africa," *Asian J. Res. Zool.*, vol. 2, no. 3, pp. 1–9, 2019.

[9] G. Hoffmann and K. Teicher, "Colorimetric method for the determination of the urease activity in soil," *Zeit. Pflanzenernaehr. Dung. Bodenkunde.*, vol. 95, p. 55, 1961.

[10] H. Kumar, V. B. Singh, B. L. Meena, S. Gaur, and R. Singla, "Paraquat poisoning: a case report," *J. Clin. Diagn. Res.*, vol. 10, no. 10, 2016.

[11] R. G. Burns, “Enzyme activity in soil,” *Soil Biol. Biochem.*, vol. 14, p. 425, 1982.

[12] C. Floch, E. Alarcon-Gutierrez, and S. Criquet, “ABTS assay of phenol oxidase activity in soil,” *J. Microbiol. Methods*, vol. 71, pp. 319–324, 2007.

[13] S. Riahi, A. B. Moghaddam, M. R. Ganjali, and P. Norouzi, “Determination of the oxidation potentials of pyrogallol and some of its derivatives: theory and experiment,” *J. Theor. Comput. Chem.*, vol. 6, pp. 331–340, 2007. M. R. Roberge, “Methodology of enzymes determination and extraction,” in *Soil Enzymes*, Academic Press, 1978, pp. 341–373.

[14] R. L. Sinsabaugh, S. D. Allison, and P. G. Donovan, “Measuring phenol oxidase and peroxidase activities with pyrogallol, L-DOPA, and ABTS: Effect of assay conditions and soil type,” *Soil Biol. Biochem.*, vol. 67, pp. 183–191, 2013.

[15] C. E. Bach, D. D. Warnock, D. J. Van Horn, and M. N. Weintraub, “Measuring phenol oxidase and peroxidase activities with pyrogallol,” *Soil Biol. Biochem.*, 2013.

[16] Z. Stępniewska, A. Wolinska, and J. Ziomek, “Response of soil catalase activity to chromium contamination,” *J. Environ. Sci.*, vol. 21, pp. 1142–1147, 2009.

[17] A. D. Vijayakumar, M. Subban, J. Jmbulingam, P. Annamalai, and P. T. Kalaichelvan, “A Rapid Sensitive Detection Method by Plate Assay for Catalase Activity from Bacterium Acinetobacter calcoaceticus AV6,” *RRJMB*, vol. 3, 2014.

[18] L. C. Blakemore, P. L. Searle, and B. K. Daly, *Methods for chemical analysis of soils*, Lower Hutt, New Zealand: New Zealand Soil Bureau, 1987, pp. 47–66.

[19] H. O. Obueh, N. Maduka, P. A. Egharevba-Ojo, K. E. Enerijiofi, and C. Ikhazuangbe-Benson, “Effect of dumpsite waste on soil, drinking water sources, and antibiotic susceptibility of isolates, in a sub-urban community, Benin city, Nigeria,” *Sci. World J.*, vol. 19, no. 3, pp. 625–633, 2024.

[20] World Health Organization, *Guidelines for drinking-water quality, incorporating 1st and 2nd Addenda, Vol. 1, Recommendations*, 3rd ed. Geneva, Switzerland: WHO, 2010.

[21] J. A. Ibiam, A. N. Oko, C. C. Amaechi, C. O. Apie, U. I. Nwali, and H. E. Isu, “Effect of waste dumpsite on the surface and groundwater supplies using water quality index in Afikpo south local government, Ebonyi state,” *World J. Adv. Res. Rev.*, vol. 21, no. 2, pp. 1343–1352, 2024, doi: 10.30574/wjarr.2024.21.2.0547.

[22] G. Bhalla, P. K. Swamee, A. Kumar, and A. Bansal, “Assessment of groundwater quality near municipal solid waste landfill by an aggregate index method,” *Int. J. Environ. Sci.*, vol. 2, no. 2, pp. 1492–1503, 2012.

[23] N. N. Odu, A. L. Omunakwe, and M. Millicent, “Comparative assessment on the physicochemical water quality of wells and boreholes in two Rivers state communities, Nigeria,” *Int. J. Res. Stud. Microbiol. Biotechnol.*, vol. 6, no. 3, pp. 5–20, 2020, doi: 10.20431/2454-9428.0603002.

[24] O. C. Nwiniyi, O. Uyi, E. J. Awosanya, I. Oyeyemi, A. M. Ugbenyen, A. Muhammad, O. A. Alabi, O. I. Ekwunife, C. O. Adetunji, and I. M. Omoruyi, “Review of drinking water quality in Nigeria: towards attaining sustainable development goal six,” *Ann. Sci. Technol.*, vol. 5, no. 2, pp. 58–77, 2020.

[25] U. U. Udofia, U. U. Udiba, L. E. Udofia, N. N. Ezike, and S. U. Udiba, “Assessment of the impact of solid waste dumps on ground water quality, Calabar municipality, Nigeria,” *J. Adv. Res. Pharm. Biol. Sci.*, vol. 2, no. 4, pp. 10–21, 2016, doi: 10.53555/nnpbs.v2i4.705.

[26] V. Samuel, W. O. M. Wilfred, V. N. Ogbonna, and V. O. Awah, “Survey of Microorganisms (Fungi) Associated with Dumpsites in Rumuolumeni, Port Harcourt, Rivers State,” *J. Biol. Genet. Res.*, vol. 10, no. 1, pp. 78–87, 2024.

[27] “The History of Bergey's Manual,” in *Bergey's Manual of Systematic Bacteriology*, 1984, pp. 1–13.

[28] E. A. Ekundayo, B. G. Olubunmi, J. K. Kone, F. O. Ekundayo, D. T. Abayomi, and H. O. Adewoyin, "Bacteriological Assessment of Soil Samples Collected from Some Selected Dump Sites in Ondo Metropolis, Ondo State, Nigeria Mercedes," *F.U.T.A. J. Life Sci.*, vol. 5, no. 1, pp. 182–189, 2025.

[29] F. C. Nireti, A. M. Adetoun, and A. O. Abayomi, "Microbiological Assessment of Soil from Dumpsites in Oduduwa University Campus," *Int. J. Sci. Adv. Innov. Res.*, vol. 3, no. 1, pp. 25–29, 2018.

[30] E. O. Ohaeri, I. Callitus, N. Linus, and O. Emmanuel, "Physicochemical Properties of Soils from Dumpsite in the Federal University of Technology, Owerri, Nigeria," *Asian J. Adv. Res. Rep.*, vol. 18, no. 12, pp. 405–411, 2024.

[31] A. Taofeek, I. A. Alexander, S. O. Simon, O. T. Jimoh, F. Suleiman, U. M. Mohammed, A. U. Roseline, O. K. Lateef, J. A. Babatunde, and S. A. Adeola, "Impact of Dumpsite Wastes on Soil Properties and Heavy Metal Concentrations in Kontagora, Nigeria," *Glob. Sci. J.*, vol. 13, no. 8, pp. 29–65, 2025.

Sinop University
Positive Science International
e-ISSN: 3108-3862

Positive Science International, 2(1), 43-52
Research Article, Year: 2026
DOI: 10.71340/psi.1709547

Evaluation of Kernel and Parameter Effects on the Performance of Classifiers for Differentiated Thyroid Cancer Recurrence

Mertcan TUTUM[1*], Yavuz ÜNAL[2]

[1]* *Graduate School of Natural and Applied Sciences, Amasya University, 05100, Amasya, Türkiye*

[2]*Department of Computer Engineering, Faculty of Engineering and Architecture, Sinop University, Sinop, Türkiye*

Article Info

Research article
Received: *30.05.2025*
Accepted: *10.06.2026*
Published: *30.06.2026*
***Corresponding Author*:** *Mertcan TUTUM*
mertutum@gmail.com
0009-0000-1292-8517
Keywords

Cancer recurrence prediction
Machine Learning
Thyroid cancer

Abstract

Thyroid cancer causes tens of thousands of deaths every year in the world. Treatment of this disease is possible with today's medical conditions. However, as in other types of cancer, recurrence is possible. The Differentiated Thyroid Cancer Recurrence dataset, which includes data from 383 patients and was obtained from the UCI platform, was used in the study. The aim of this study is to compare the classification performances of machine learning algorithms according to various parameters and Kernel functions in order to predict recurrence in thyroid cancer patients. For this purpose, three machine learning algorithms were used to predict differentiated thyroid cancer recurrence. In the K-Nearest Neighbors (K-NN) algorithm, the most appropriate k parameter was determined by trying different neighbor number (k) values. The Support Vector Machines (SVM) algorithm examined various kernel functions and hyperparameter settings. In addition, model performance was compared by optimizing different tree numbers and depth parameters with the Random Forest algorithm. These methods aimed to determine the model with the highest accuracy and generalization capacity.

Farklılaşmış Tiroid Kanseri Nüksü İçin Sınıflandırıcıların Performansı Üzerindeki Çekirdek ve Parametre Etkilerinin Değerlendirilmesi

Makale Bilgisi

Araştırma makalesi
Başvuru: *30.05.2025*
Kabul: *10.06.2026*
Yayın: *30.06.2026*
***Sorumlu Yazar*:** *Mertcan TUTUM*
mertutum@gmail.com
0009-0000-1292-8517
Anahtar Kelimeler

Kanser tekrarlama tahmini
Makine Öğrenimi
Tiroid kanseri

Özet

Tiroid kanseri, dünyada her yıl on binlerce kişinin ölümüne neden olmaktadır. Günümüzün tıbbi imkânlarıyla bu hastalığın tedavisi mümkündür. Ancak, diğer kanser türlerinde olduğu gibi, nüksetme olasılığı da mevcuttur. Çalışmada, UCI platformundan elde edilen ve 383 hastanın verilerini içeren "Farklılaşmış Tiroid Kanseri Nüksü" veri seti kullanılmıştır. Bu çalışmanın amacı, tiroid kanseri hastalarında nüksü tahmin etmek için çeşitli parametrelere ve çekirdek fonksiyonlarına göre makine öğrenimi algoritmalarının sınıflandırma performanslarını karşılaştırmaktır. Bu amaçla, farklılaşmış tiroid kanseri nüksünü tahmin etmek üzere üç makine öğrenimi algoritması kullanılmıştır. K-En Yakın Komşu (K-NN) algoritmasında, farklı komşu sayısı (k) değerleri denenerek en uygun k parametresi belirlenmiştir. Destek Vektör Makineleri (SVM) algoritmasında çeşitli çekirdek fonksiyonları ve hiperparametre ayarları incelenmiştir. Ayrıca, Rastgele Orman algoritmasıyla farklı ağaç sayısı ve derinlik parametreleri optimize edilerek model performansı karşılaştırılmıştır. Bu yöntemler, en yüksek doğruluk ve genelleme kapasitesine sahip modeli belirlemeyi amaçlamıştır.

To cite this article:
Tutum, M., Ünal Y. (2026). Evaluation of Kernel and Parameter Effects on the Performance of Classifiers for Differentiated Thyroid Cancer Recurrence, Positive Science International, 2(1), 43-52, https://doi.org/10.71340/psi.1709547

1. Introduction

In recent years, the incidence of thyroid cancer has been rapidly increasing. The advancements in imaging technologies have enabled the early diagnosis of this disease. The survival rate is quite high compared to other types of cancer. Thyroid cancer is a cancerous tumor that starts in the thyroid gland in the front of the neck [1]. It happens when cells in this gland, which are vital for making thyroid hormones, grow out of control. Papillary thyroid carcinoma is the most frequent type of thyroid cancer. It makes up around 80% of all cases and usually has a decent prognosis [2]. Follicular thyroid cancer is not as frequent as papillary thyroid cancer, but it can be treated in the same way. The C cells in the thyroid give rise to medullary thyroid carcinoma, which may be linked to genetics [3, 4].

In the last few years, a growing number of people have been getting thyroid cancer. By modelling the stages of thyroid cancer spreading to the body, the risk of death for the patient can be lowered. When the main risk factors for the disease are known, early diagnosis and treatment planning can help steer the disease in the right direction.

Differentiated Thyroid Carcinoma (DTC), notably the papillary and follicular subtypes, is a kind of cancer that usually has a good prognosis and a five-year survival rate of over 95%. But even if this is a benign course, the rate of recurrence (reappearance) is still quite high [5, 6].

Machine learning is changing a lot of things in health care, such how doctors diagnose, treat, and follow up with patients. It works well for finding diseases early and figuring out risk factors, especially when it finds meaningful patterns in vast data sets. Image processing techniques have made it possible to automatically find cancer and other disorders. Also, machine learning algorithms play a big role in making personalized treatment plans and medication development processes. Analyzing electronic health records makes health services better and more efficient. So, machine learning is now a very important tool in the health field for lowering costs and improving patient outcomes [7].

The aim of this study is to predict recurrence in patients with DTC by comparing the classification performance of machine learning algorithms, specifically Support Vector Machines (SVM) and K-Nearest Neighbors (K-NN). The study further investigates the impact of different kernel functions (e.g., RBF, Polynomial) and parameter settings on model accuracy to identify the most effective predictive configuration.

Machine learning has become a common tool for predicting thyroid cancer outcomes, with studies focusing on both survival analysis and recurrence prediction. The following studies illustrate the range of approaches applied to clinical and pathological data in this field.

Mourad et al. [8] proposed a machine learning approach to predict survival in thyroid cancer patients, combining 34 clinical variables from the SEER database with feature selection methods such as Fisher discriminant ratio, Kruskal-Wallis analysis, and Relief-F. They trained multilayer perceptron-based supervised neural networks with patient groups ranging from 6,756 to 20,344 and achieved 94.5%

accuracy in distinguishing patients who lived longer than 10 years from diagnosis from those who died within five years.

Park and Lee [1] analyzed clinicopathological data from 1040 patients diagnosed with papillary thyroid carcinoma (PTC) between 2003 and 2009 to predict disease recurrence and developed a machine learning-based prediction model. They compared the performance of five different machine learning models using parameters such as age, gender, tumor size, ETE, ENE, pT, pN, number of metastatic lymph nodes, and lymph node ratio (LNR). The Decision Tree model achieved the highest accuracy at 95%, while the lightGBM and stacking models showed 93% accuracy.

Kim et al. [2] proposed an inductive logic programming-based approach to predict recurrence in papillary thyroid cancer patients who underwent thyroidectomy. They used data from 785 patients who underwent bilateral total thyroidectomy and received radioactive iodine therapy; 624 (79.5%) were allocated for rule generation and 161 (20.5%) for validation, and the analysis was performed using the DELMIA Process Rules Discovery tool. They identified three rules that predicted recurrence and determined that postoperative thyroglobulin levels were the strongest predictor. The rules generated in the validation set correctly predicted 10 out of 14 recurrence cases, achieving a 71.4% success rate.

Lee and Park [9] compiled the recent use of machine learning methods in the early diagnosis of thyroid diseases according to different data types. They determined that random forest and gradient boosting methods were the most suitable approaches for numerical data, while random forest was the most suitable approach for genomic and ultrasound data. In the studies examined, they reported that accuracy values ranged from 64.3% to 99.5%, sensitivity from 66.8% to 90.1%, specificity from 61.8% to 85.5%, and the area under the ROC curve from 64.0% to 96.9%. They identified clinical stage, histological type, age, tumor diameter, extrathyroidal spread, various RNA and microRNA expression levels, and ultrasound characteristics as the most important variables for early diagnosis.

Zhang et al. [10] systematically compiled machine learning-based applications used in the pathogenesis, diagnosis, and prognosis of thyroid cancer and created a comprehensive taxonomy. By reviewing a total of 758 studies, they classified artificial intelligence techniques in the field and revealed the organizational structure of the existing literature. They identified key challenges encountered in thyroid cancer research and suggested future research opportunities for less studied topics.

Duan et al. [11] applied machine learning algorithms to predict hypothyroidism developing in Graves' disease patients after radioactive iodine therapy (RAI) at an early stage. They randomly divided 471 patients who underwent RAI between 2016 and 2019 into two groups: 310 for training and 161 for validation. They extracted 138 clinical and laboratory features from electronic medical records. They developed a multivariate model including patient age, thyroid mass, 24-hour radioactive iodine uptake, aspartate aminotransferase, thyroid antibodies, and neutrophil count. They obtained an AUROC value of 0.72 in the training set and 0.74 in the validation set, along with an F1 score of 0.74 and an MCC score of 0.63 in both sets and created a nomogram for clinical use.

2. Methods

2.1. Dataset

In our study, the Differentiated Thyroid Cancer Recurrence dataset obtained from the University of California Irvine (UCI) Machine Learning Repository website was used [12]. The features and their types included in the dataset are provided in Table 1.

Table 1. Differentiated thyroid cancer recurrence dataset and features

Feature name	Role	Type
Age	Feature	Integer
Gender	Feature	Categorical
Smoking	Feature	Categorical
Hx Smoking	Feature	Categorical
Hx Radiothreapy	Feature	Categorical
Thyroid Function	Feature	Categorical
Physical Examination	Feature	Categorical
Adenopathy	Feature	Categorical
Pathology	Feature	Categorical
Focality	Feature	Categorical
Risk	Feature	Categorical
T	Feature	Categorical
N	Feature	Categorical
M	Feature	Categorical
Stage	Feature	Categorical
Response	Feature	Categorical
Recurrend	Target	Categorical

The dataset consists of 16 features and one target. These include information such as the patient's age, gender, whether they smoke or not, whether they undergo radiotherapy or not, and whether they engage in physical activity or not. Out of these 16 features, 15 are categorical, and one is an integer.

2.2. Parameter Optimization

In machine learning, parameter optimization refers to modifying a model's learnable parameters or hyperparameters to maximize its performance throughout the training phase. The weights and bias values that the model learns during training are called parameters; the coefficients in linear regression are one example. The learning rate, the number of network layers, and the batch size are examples of hyperparameters, which are the values that are set before training and that dictate the model's structure.

To reduce the model's loss, the Gradient Descent method enables the parameters to be modified in accordance with the gradients. While hyperparameter optimization can employ trial-and-error techniques like Grid Search and Random Search, Bayesian Optimization uses a probabilistic approach to determine the optimal hyperparameters [13]. By automating this process, autoML tools Optuna and Hyperopt are two examples that make hyperparameter optimization easier. Generally speaking, the goal is to improve performance, reduce training and test error, or prevent overfitting in order to increase the model's capacity for generalization [13].

2.3. Support Vector Machine

One supervised learning method that is well-known for its excellent performance, particularly in classification tasks, is Support Vector Machines (SVM). Finding a "hyperplane" (decision boundary) that best divides data points from different classes is its primary objective; in the process, it concentrates on maximizing the "margin," or distance, between the data points closest to this hyperplane, known as "support vectors." By improving the model's capacity for generalization, maximizing the margin enables it to produce predictions on fresh, untested data that are more accurate. Because SVMs can use a technique known as the "kernel trick" to transfer complex data structures that cannot be separated linearly to a higher dimensional space and make linear distinctions there, they also provide flexibility [14] [15] [16].

2.4. Random Forest

One supervised learning algorithm that can yield good results, particularly in complex data sets, is Random Forest. It is essentially predicated on the idea that a "forest" is created when numerous decision trees converge. Using distinct subsets and features chosen at random from the primary data set, each tree is trained separately throughout the training process. Every tree in the forest makes a prediction when one is needed, and the class that receives the most votes (in classification problems) or the average of the tree predictions (in regression problems) is the final outcome. By decreasing the propensity of a single decision tree to overfit the data (overfitting), this collective decision-making mechanism improves the model's capacity for generalization and typically yields more reliable and accurate predictions [17] [18].

2.5. K-Nearest Neighbours (K-NN) algorithm

The k-Nearest Neighbours (k-NN) algorithm is one of the easiest and most common ways to classify things in supervised learning. The main idea behind it is to find the distances between the sample to be classed and the data as the number of nearest neighbours k in the feature space. The Euclidean distance metric is the most common one, although for some sorts of problems, other distance metrics like Manhattan and Minkowski may be better. k-NN is quite sensitive to how its parameters are adjusted. The right k value has a direct effect on how well the model works. Small k values can make the model too specific, while very large k values can make it harder for the model to generalize. Also, the k-NN technique is easy to train, and all the math is done when the data is classified, therefore it can be expensive to run on large data sets. The k-NN technique is good for medical classification issues like

predicting the recurrence of thyroid cancer because it makes proper classifications by looking at the local structure of the instances in the data set [19].

2.6. WEKA

The University of Waikato in New Zealand created the well-known open-source machine learning program Weka (Waikato Environment for Knowledge Analysis). Weka provides an extensive toolkit for data mining and machine learning algorithms and is written in the Java programming language. Numerous machine learning tasks, including feature selection, regression, clustering, classification, and data preprocessing, are supported. Its intuitive graphical user interface makes data analysis simple, even for users without programming experience. Weka, which is widely used in both academia and business, can work with various data formats, including CSV and Excel, and supports the ARFF (Attribute-Relation File Format) format. Numerous algorithms, including k-means clustering, decision trees, neural networks, support vector machines, and others, are included, and the results can be visualized [20] [21].

2.7. Performance Metrics

The study's performance has been evaluated using a variety of criteria. These criteria include F1-score, recall, accuracy, and precision. The ideas of true positive, true negative, false positive, and false negative must be understood before the formulas for these terms can be explained. True positives are examples that are correctly classified as positive, true negatives are examples that are correctly classified as negative, false positives are examples that are incorrectly classified as positive, and false negatives are examples that are incorrectly classified as negative [22] [24]. Consequently, the following formulas are given for the performance metrics:

$$Accuracy = \frac{\mathrm{TP+TN}}{\mathrm{TP+TN+FP+FN}} \quad (1)$$

$$Precision = \frac{\mathrm{TP}}{\mathrm{TP+FP}} \quad (2)$$

$$Recall = \frac{\mathrm{TP}}{\mathrm{TP+FN}} \quad (3)$$

$$f1 - score = 2x\frac{\mathrm{PrecisionxRecall}}{\mathrm{Precision+Recall}} \quad (4)$$

3. Results and Discussion

The analyses were performed on the WEKA program. CSV format is one of the formats that can be used in the WEKA program. Model parameters and kernel types were tested randomly and in various combinations for performance evaluation. First, the Support Vector Machine (SVM) classifier was used and the kernel functions were tested as RBF, Polynomial Kernel, Normalized Polynomial Kernel and PUK, respectively. The results are given in Table 2.

Table 2. Comparison of Support Vector Machine (SVM) classifier performance using different kernel functions

Classifier	Kernel	Accuracy	Precision	Recall	F1-score
SVM	RBF	94.57%	0.94	0.94	0.94
	PolyKernel	95.56%	0.95	0.95	0.95
	NormalizedPolyKernel	94.77%	0.94	0.94	0.94
	Puk	93.22%	0.93	0.93	0.93

When the accuracy results obtained by using different kernel functions in the Support Vector Machine (SVM) algorithm are examined, Polynomial Kernel has shown superior performance than other kernel types with the highest success rate (95.56%). While RBF and Normalized Polynomial Kernel have similar accuracy values (94.57% and 94.44%), PUK kernel has lower performance compared to the others (93.22%). These findings show that the kernel selection has a significant effect on the model success. The classification results obtained with K-NN and different k values are given in Table 3

Table 3. Performance evaluation of the K-Nearest Neighbors (K-NN) classifier with varying values of K.

Classifier	K	Accuracy	Precision	Recall	F1-score
K-NN	1	91.38%	0.91	0.91	0.91
	2	92.95%	0.93	0.93	0.92
	3	93.21%	0.93	0.93	0.93
	4	93.47%	0.93	0.93	0.93

The effect of different k values on model performance in the K-Nearest Neighbors (K-NN) algorithm was investigated. As a result of the experiments, 91.38% accuracy rates were obtained for k=1, 92.95% for k=2, 93.21% for k=3 and 93.47% for k=4. These findings show that there is a certain improvement in classification accuracy with increasing k values; however, it should be noted that the increase may stop or start to decrease after a certain point. Therefore, the optimal k value should be selected carefully. The classification results obtained with the Random Forest classifier using different numbers of trees are presented in Table 4.

Table 4. Impact of the number of trees on the performance of the Random Forest classifier

Classifier	Num. of Trees	Accuracy	Precision	Recall	F1-score
Random Forest	10	96.34%	0.96	0.96	0.96
	50	96.86%	0.96	0.96	0.96
	100	96.34%	0.96	0.96	0.96
	200	96.34%	0.96	0.96	0.96

The effect of different tree numbers on model success was evaluated in the Random Forest algorithm. Accuracy rates of 96.34% were obtained with 10 trees, 96.86% with 50 trees, and 96.34% with 100 and 200 trees. The results show that a small performance increase was achieved by increasing the number of trees to 50, but adding more trees did not lead to a significant improvement in accuracy. This situation reveals that when the optimal number of trees is exceeded, the model complexity increases and the performance becomes stagnant.

Random Forest gave the highest accuracy at 96.86% with 50 trees, followed by SVM with Polynomial kernel at 95.56% and K-NN at 93.47%. The dataset structure explains this ordering. Sixteen of seventeen features are categorical, and tree-based methods split categorical attributes directly while SVM and K-NN depend on distance metrics that distort under encoded categories.

Borzooei et al. [25] reported similar accuracy ranges on the same 383 patient cohort, which suggests classical machine learning has likely reached its ceiling on this dataset. Adding trees beyond 50 produced no gain, and kernel differences in SVM stayed within one percentage point. Smaller models are preferable for clinical use because they train and run faster.

Several limitations apply. The class distribution was not reported, and no resampling or class weighting was used, so accuracy may overstate performance on the recurrence class. ROC AUC, sensitivity, specificity, and confusion matrices would have given a fuller picture. The K-NN experiments stopped at k=4 and used Euclidean distance, which is suboptimal for categorical data. External validation on independent cohorts is also missing, so the results describe one dataset rather than a clinical tool.

4. Conclusion

This study looked at how well three machine learning algorithms Support Vector Machine (SVM), K-Nearest Neighbours (K-NN), and Random Forest could predict the return of differentiated thyroid carcinoma in individuals. We looked at multiple kernel functions for SVM and varied parameter settings for K-NN and Random Forest to find the best model accuracy. The results showed that Polynomial Kernel had the best accuracy of all the SVM kernels. K-NN, on the other hand, got better as the K values went up to 4. Random Forest worked well with 50 trees, but there were no big improvements after that.

These results show how important it is to use the right kernel and tune the hyperparameters to make medical classification tasks more accurate. The study shows that machine learning models could be useful for finding cancer recurrences early, which could help doctors give each patient the best care possible. Different research might look at different algorithms and use bigger, more varied datasets to make the model even more useful in the real world and for more people.

Next steps include comparing gradient boosting methods (XGBoost, LightGBM, CatBoost), since CatBoost handles categorical variables natively. SHAP analysis will quantify which clinical features drive predictions, which is more actionable for physicians than accuracy alone. External

validation on multi center Turkish cohorts will test transferability. Deep tabular models such as TabNet and FT Transformer are worth comparing against the ensemble baselines established here.

On the methodological side, class imbalance will be handled with SMOTE and class weighted loss, hyperparameter search will move from manual WEKA testing to Optuna under nested cross validation, and the evaluation protocol will expand to ROC AUC, precision recall curves, and Matthews correlation coefficient.

Declarations

Funding/Financial Disclosure The authors have no received any financial support for the research, authorship, or publication of this study.

Ethics Committee Approval and Permissions The work does not require ethics committee approval and any private permission.

Conflict of Interests The authors stated that there is no conflict of interest in this article.

References

[1] Y. M. Park and B.-J. Lee, "Machine learning-based prediction model using clinico-pathologic factors for papillary thyroid carcinoma recurrence," *Sci. Rep.*, vol. 11, no. 1, p. 4948, Mar. 2021, doi: 10.1038/s41598-021-84504-2.

[2] S. Y. Kim et al., "New approach of prediction of recurrence in thyroid cancer patients using machine learning," *Medicine*, vol. 100, no. 42, p. e27493, Oct. 2021, doi: 10.1097/MD.0000000000027493.

[3] İ. Kara, M. G. Yildiz, and İ. Orhan, "Tiroid Nodülü," *Kahramanmaraş Sütçü İmam Üniversitesi Tıp Fakültesi Dergisi*, vol. 15, no. 3, pp. 94–99, Oct. 2020, doi: 10.17517/ksutfd.685884.

[4] H. Wang et al., "Development and validation of prediction models for papillary thyroid cancer structural recurrence using machine learning approaches," *BMC Cancer*, vol. 24, no. 1, p. 427, Apr. 2024, doi: 10.1186/s12885-024-12146-4.

[5] B. Bektas Gunes, R. Samlı, M. B. Dogan, and D. Yildirim, "SEGMENTATION OF THYROID NODULES ON ULTRASOUND IMAGES," *J. Naval Sci. Eng.*, vol. 20, no. 2, pp. 191–211, Nov. 2024, doi: 10.56850/jnse.1507140.

[6] L.-R. Li, B. Du, H.-Q. Liu, and C. Chen, "Artificial Intelligence for Personalized Medicine in Thyroid Cancer: Current Status and Future Perspectives," *Front. Oncol.*, vol. 10, p. 604051, Feb. 2021, doi: 10.3389/fonc.2020.604051.

[7] Z. Aytaç, İ. Iseri, and B. Dandil, "Derin Öğrenme Kullanarak Tiroid Kanseri Teşhisi," *Eur. J. Sci. Technol.*, Dec. 2021, doi: 10.31590/ejosat.1011166.

[8] M. Mourad et al., "Machine Learning and Feature Selection Applied to SEER Data to Reliably Assess Thyroid Cancer Prognosis," *Sci. Rep.*, vol. 10, no. 1, p. 5176, Mar. 2020, doi: 10.1038/s41598-020-62023-w.

[9] K.-S. Lee and H. Park, "Machine learning on thyroid disease: a review," *Front. Biosci. (Landmark Ed)*, vol. 27, no. 3, p. 101, Mar. 2022, doi: 10.31083/j.fbl2703101.

[10] X. Zhang, V. C. Lee, and F. Liu, "From Data to Insights: A Comprehensive Survey on Advanced Applications in Thyroid Cancer Research," 2024, *arXiv*, doi: 10.48550/ARXIV.2401.03722.

[11] L. Duan et al., "Machine learning identifies baseline clinical features that predict early hypothyroidism in patients with Graves' disease after radioiodine therapy," *Endocr. Connect.*, vol. 11, no. 5, p. e220119, May. 2022, doi: 10.1530/EC-22-0119.

[12] S. Borzooei, G. Briganti, M. Golparian, J. R. Lechien, and A. Tarokhian, “Machine learning for risk stratification of thyroid cancer patients: a 15-year cohort study,” *Eur. Arch. Otorhinolaryngol.*, vol. 281, no. 4, pp. 2095–2104, Apr. 2024, doi: 10.1007/s00405-023-08299-w.

[13] C. Parlak, “Konuşma Duygu Tanıma Uygulamalarında Hiper Parametre Optimizasyonu ile Derin Öğrenme Metotlarının Geliştirilmesi,” *Karadeniz Fen Bilimleri Dergisi*, vol. 14, no. 4, pp. 1955–1975, Dec. 2024, doi: 10.31466/kfbd.1508578.

[14] S. Metlek and K. Kayaalp, “Derin Öğrenme ve Destek Vektör Makineleri İle Görüntüden Cinsiyet Tahmini,” *Düzce Üniversitesi Bilim ve Teknoloji Dergisi*, vol. 8, no. 3, pp. 2208–2228, Jul. 2020, doi: 10.29130/dubited.707316.

[15] G. Harman, “Destek Vektör Makineleri ve Naive Bayes Sınıflandırma Algoritmalarını Kullanarak Diabetes Mellitus Tahmini,” *Eur. J. Sci. Technol.*, Dec. 2021, doi: 10.31590/ejosat.1041186.

[16] E. Efeoğlu, “Destek Vektör Makinelerinin Wi-Fi Tabanlı İç Mekan Lokalizasyon Tespitinde Kullanımı ve Çekirdek Fonksiyon Seçiminin Sınıflandırma Performansına Etkisi,” *Osmaniye Korkut Ata Üniversitesi Fen Bilimleri Enstitüsü Dergisi*, vol. 5, no. 3, pp. 1370–1382, Dec. 2022, doi: 10.47495/okufbed.1057825.

[17] O. K. M. Salman and B. Aksoy, “RASGELE ORMAN VE İKİLİ PARÇACIK SÜRÜ ZEKÂSI YÖNTEMİYLE KALP YETMEZLİĞİ HASTALIĞINDAKİ ÖLÜM RİSKİNİN TAHMİNLENMESİ,” *Int. J. 3D Print. Technol. Dig. Ind.*, vol. 6, no. 3, pp. 416–428, Dec. 2022, doi: 10.46519/ij3dptdi.982670.

[18] H. Y. Dalkiliç, S. N. YeşiLyurt, and P. Samui, “Daily Flow Modeling With Random Forest and K-Nearest Neighbor Methods,” *Erzincan Üniversitesi Fen Bilimleri Enstitüsü Dergisi*, vol. 14, no. 3, pp. 914–925, Dec. 2021, doi: 10.18185/erzifbed.949126.

[19] Ö. Türk, “MR GÖRÜNTÜLERİNDEN ALZHEİMER TESPİTİNDE BOYUT AZALTMA VE DERİN ÖĞRENME YAKLAŞIMLARININ KARŞILAŞTIRILMASI,” *DÜMF MD*, Sep. 2022, doi: 10.24012/dumf.1141233.

[20] M. Hacibeyoglu, M. ÇeliK, and Ö. Erdaş ÇiÇek, “K En Yakın Komşu Algoritması ile Binalarda Enerji Verimliliği Tahmini,” *neufmbd*, no. 2, Dec. 2023, doi: 10.47112/neufmbd.2023.10.

[21] A. V. Ağlarcı and F. Karakurt, “K En Yakın Komşu Makine Öğrenme Algoritmasına Dayalı Diabetes Mellitus Tahmini,” *Turk J. Diab. Obes.*, vol. 8, no. 3, pp. 265–276, Dec. 2024, doi: 10.25048/tudod.1549498.

[22] Ö. F. Akmeşe, “Diagnosing Diabetes with Machine Learning Techiques,” *Hittite J. Sci. Eng.*, vol. 9, no. 1, pp. 9–18, Mar. 2022, doi: 10.17350/HJSE19030000250.

[23] M. DiRiK, “Machine learning-based lung cancer diagnosis,” *Turk. J. Eng.*, vol. 7, no. 4, pp. 322–330, Oct. 2023, doi: 10.31127/tuje.1180931.

[24] Y. Unal and M. Bolat, “Detecting Wheat Leaf Diseases: A Deep Feature-Based Approach with Machine Learning Classification,” *SJAFS*, no. 3, Dec. 2024, doi: 10.15316/SJAFS.2024.041.

[25] D. Bhende et al., “Machine Learning-Based Classification of Thyroid Disease: A Comprehensive Study on Early Detection and Risk Factor Analysis,” in *Proc. IEEE Int. Students’ Conf. Electr. Electron. Comput. Sci. (SCEECS)*, Bhopal, India, Feb. 2024, pp. 1–6, doi: 10.1109/SCEECS61402.2024.10481980.

Sinop University
Positive Science International
e-ISSN: 3108-3862

Positive Science International, 2(1), 53-71
Research Article, Year: 2026
DOI: 10.71340/psi.1710774

The Role of Wireless Sensor Networks in Military Operations: A Survey

Erhan SESLİ[1*]

[1*]*Karadeniz Technical University, Of Technology Faculty, Electronics and Telecommunication Engineering, Trabzon, Türkiye*

Article Info

Review article
Received: *31.05.2025*
Accepted: *11.06.2026*
Published: *30.06.2026*
***Corresponding Author*:** *Erhan SESLİ*
erhansesli@ktu.edu.tr
0000-0002-0039-2927
Keywords

Wireless Sensor Networks, Military Applications, Surveillance Systems, Battlefield Monitoring.

Abstract

Wireless Sensor Networks (WSNs) are today key technology of contemporary military applications due to their cost-effectiveness, scalability, and ability to support real-time operations. WSNs are widely used in military applications for intelligence, surveillance, reconnaissance, environmental monitoring, and battlefield awareness thanks to the spatially distributed autonomous sensor nodes that sense, process, and transmit important information. Consequently, these networks provide enhanced decision support, minimize operational risks, and improve mission accomplishment. Despite their inherent advantages, the deployment of WSNs in hostile and dynamic military environments faces many challenges. Security, privacy, fault tolerance, real-time operation, scalability, and self-organization are of utmost importance in this respect. Furthermore, energy efficiency, node mobility, data reliability, and attack tolerance are key factors influencing their operational usability. Current research has proposed various solutions, like AI-integrated data processing, blockchain-based security mechanisms, and bio-inspired optimization algorithms to address the above issues. The aim of this work is to provide a detailed overview of the application of WSNs in military operations, their building blocks, types of applications, and operational requirements. It also explains the state-of-the-art technology development at present and critically examines existing solutions to overcome main limitations. Through the examination of the recent, and future works, this research offers a better comprehension of how WSNs can evolve into more adaptive, secure, and effective military systems. The research findings are expected to serve as a roadmap for researchers and practitioners who seek to design next-generation military sensor networks.

Askeri Operasyonlarda Kablosuz Sensör Ağlarının Rolü: Bir Araştırma

Makale Bilgisi

Derleme makale
Başvuru: *31.05.2025*
Kabul: *11.06.2026*
Yayın: *30.06.2026*
***Sorumlu Yazar*:** *Erhan SESLİ*
erhansesli@ktu.edu.tr
0000-0002-0039-2927
Anahtar Kelimeler

Kablosuz Algılayıcı Ağları, Askeri Uygulamalar, Gözetim Sistemleri, Savaş Alanı İzleme.

Özet

Kablosuz Algılayıcı Ağları (KAA), maliyet etkinliği, ölçeklenebilirliği ve gerçek zamanlı operasyonları destekleme yeteneği nedeniyle günümüz askeri uygulamalarının temel teknolojilerinden biridir. KAA'lar, önemli bilgileri algılayan, işleyen ve ileten, mekânsal olarak dağıtılmış otonom algılayıcı düğümleri sayesinde istihbarat, gözetim, keşif, çevre izleme ve savaş alanı farkındalığı için askeri uygulamalarda yaygın olarak kullanılmaktadır. Sonuç olarak, bu ağlar gelişmiş karar desteği sağlar, operasyonel riskleri en aza indirir ve görev başarısını artırır. Doğal avantajlarına rağmen, KAA'ların düşmanca ve dinamik askeri ortamlarda konuşlandırılması birçok zorlukla karşı karşıyadır. Bu bağlamda güvenlik, gizlilik, hata toleransı, gerçek zamanlı çalışma, ölçeklenebilirlik ve kendi kendine organizasyon son derece önemlidir. Ayrıca, enerji verimliliği, düğüm hareketliliği, veri güvenilirliği ve saldırı toleransı, operasyonel kullanılabilirliklerini etkileyen temel faktörlerdir. Mevcut araştırma çalışmaları, yukarıdaki sorunları ele almak için yapay zeka bütünleşmiş veri işleme, blok zinciri tabanlı güvenlik mekanizmaları ve biyolojik ilhamlı optimizasyon algoritmaları gibi çeşitli çözümler önermiştir. Bu çalışmanın amacı, KAA'ların askeri uygulamalardaki kullanımına, yapı taşlarına, uygulama türlerine ve operasyonel gereksinimlerine dair ayrıntılı bir genel bakış sunmaktır.

Ayrıca, günümüzdeki en son teknoloji gelişimini açıklamakta ve temel sınırlamaların üstesinden gelmek için mevcut çözümleri eleştirel bir şekilde incelemektedir. Son ve gelecekteki çalışmaları inceleyerek, bu araştırma, KAA'ların nasıl daha uyarlanabilir, güvenli ve etkili askeri sistemlere dönüşebileceğine dair daha iyi bir anlayış sunmaktadır. Araştırma bulgularının, yeni nesil askeri algılayıcı ağları tasarlamak isteyen araştırmacılar ve uygulayıcılar için bir yol haritası görevi görmesi beklenmektedir

To cite this article:
Sesli, E. (2026). The Role of Wireless Sensor Networks in Military Operations: A Survey, Positive Science International, 2(1), 53-71, https://doi.org/10.71340/psi.1710774

1. Introduction

WSNs are autonomous networks of spatially distributed sensor nodes with sensing, processing, and wireless communicating capabilities [1], [2]. WSNs cover a vast spectrum of applications such as environmental monitoring, industrial automation, smart cities, military, etc., [1], [3], [4]. WSNs operate under the principle that nodes sensing environmental data (temperature, humidity, pressure and motion etc) distribute such data, process it, and in most cases, send it to the gateway through a multi-hop communication scheme [1], [3]. Energy efficiency, scalability, and fault-tolerance are critical factors in the design of these systems [2], [5].

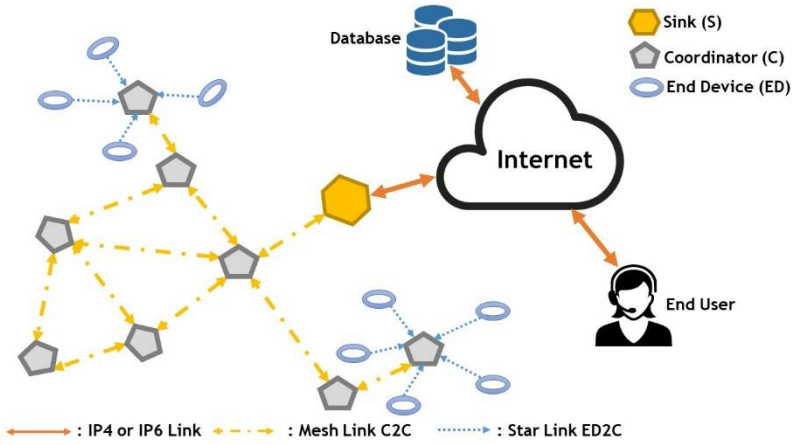

Figure 1. A traditional WSN scheme (Created by the author)

In Figure 1 the fundamental components of WSNs can be seen clearly. Sensor nodes represented by the elliptical shape in the figure, which perceive environment information and do not have enough capability of processing, are known as End Devices (EDs). EDs in WSNs are classed as Reduced-Function Devices (RFD). EDs relay the data they receive from the environment to nodes known as Coordinators (C) with advanced capabilities in the coverage area through the establishment of a star topology connection. Coordinators are known as Full Function Devices (FFD) because they can send information to nodes that share similar features and communicate using a specific protocol, among other capabilities. They use a mesh topology to interact with one another and ultimately relay information to

the Sink (S) node, which acts as a gateway and possesses FFD characteristics. The Sink then transmits this information to the internet, where it can reach a relevant database or end user [1], [3].

WSNs are increasingly becoming pertinent for civil and military applications due to their ability for low-cost installation, ability for real-time information collection and architectural scalability [1], [2], [6]. In civilian contexts, WSNs are used in a variety of fields, such as environmental monitoring, smart city infrastructure, enhancing agricultural crop yields, remote patient monitoring in healthcare, and disaster alert systems [1], [2], [6]. Especially their incorporation with the Internet of Things (IoT) renders the networks more accessible and functional in daily life.

From a strategic perspective, WSNs provide critical benefits in crucial military operations like border security, battlefield surveillance, tracking enemy movements, intelligence gathering, and mine detection [3], [6], [7], [8], [9]. The main reasons for their use in this area can be summed up as being cost-effective, stealthy in operation, capable of remote surveillance, reducing the risk of personnel casualties, and improving situational awareness [3], [6], [7].

Unlike traditional surveillance and communication systems, WSNs can be quickly and economically deployed over large areas and can operate autonomously [3], [6], [7]. While manned reconnaissance activities, especially in areas where hostile elements are present, involve serious security risks, WSN-based solutions minimize this risk and increase personnel safety [3], [9]. Thanks to the compact size of the sensor nodes and their low energy consumption, these systems can operate unnoticed for extended periods, providing a significant edge in stealth during military operations [2], [5], [9]. Additionally, with remote monitoring capabilities, real-time information can be gathered from hard-to-reach and hazardous areas, boosting the situational awareness of military units and enhancing decision-making processes [2], [3], [9].

Thanks to their versatile benefits, WSNs have become an indispensable component in modern military operations at both strategic and tactical levels [3], [7], [9]. These technologies play an important role in the realization of many critical tasks such as providing real-time information on the battlefield, early detection of threats, increasing border security and supporting complex operations. However, the special requirements and challenges for WSN applications in military environments necessitate different approaches in the design and implementation of these systems. It is precisely these challenges that motivate the present study; accordingly, the main contributions of this work are summarized as follows:

- A systematic categorization of WSN applications in military operations considering their operating environments and particular needs is made.
- Important issues related to military operations, such as energy limitations (e.g., Energy Hole problem), reliability of the network, accuracy of positioning, and numerous security threats are considered thorough.
- Recently introduced state-of-the-art techniques used in addressing these problems, including the use of Artificial Intelligence (AI) based monitoring systems, blockchain for secure routing, and bio-inspired optimization techniques are discussed and compared.

- Research gaps and possible future directions such as Internet of Battlefield Things (IoBT) and federated learning are presented to inspire other researchers to develop future tactical networks.

In order to maintain transparency and repeatability, the sub-section below provides information about the methodology employed throughout the survey, which includes the database search procedure, the inclusion-exclusion criteria employed, and the paper selection process.

1.1. Survey Methodology

In order to systematically present the contributions of WSNs within the military field, a systematic search process was carried out for collecting and reviewing the scientific literature. The search process was based on academic literature sources such as IEEE Xplore, ScienceDirect, SpringerLink, and Google Scholar literature databases. For identifying relevant scientific literature, the following combination of keywords was used: ("wireless sensor networks" OR "WSN") AND ("military applications" OR "battlefield surveillance" OR "defense and security"). The scope of the searched articles was between 2008 and 2026, with particular attention paid to the latest developments in the last five years to cover state-of-the-art technologies, including AI and Blockchain. Peer-reviewed journals, scientific proceedings, and defense technology reports in the English language were considered. The exclusion criteria was determined as articles with only civilian use of wireless sensor networks with no military potential, non-English papers and scientific literature without verification. The first search process resulted in 1810 records. After removing duplicate entries and studies outside the scope of military WSN applications, the detailed title and abstract screening were performed. After this initial screening stage, 40 articles were selected for full text assessment. Finally, 26 studies were selected according to the inclusion and exclusion criteria and considered as the main sources for this survey.

2. Wireless Sensor Networks in Military Field

The main elements that stand out in the wireless sensor network (WSN) applications in the military field are the wireless architectural structures used, military sensor technologies, secure communication mechanisms and advanced data processing strategies. In this section, these elements are discussed in detail.

2.1. System Architecture

Military WSNs can be designed with different architectural structures depending on operational requirements, mission type and the characteristics of the land where wireless nodes will be deployed. The basic communication approach is that nodes deliver data directly to a central point (single-hop) or by transmitting via other nodes (multi-hop) [6]. Multi-hop communication provides the opportunity to cover wider areas and overcome obstacles, but it brings with it difficulties such as routing complexity and energy consumption [3], [6]. It is possible to divide the architectural approaches in WSNs into three parts. The first is the structure called Hierarchical architecture. End nodes (EDs) which are the RFDs collect data, while coordinator nodes (C) which are FFDs and have higher processing capabilities,

undertake data aggregation and routing tasks. This model facilitates scalability and administration of the network [3], [7]. The other architecture is cluster-based. The sensor nodes are partitioned into clusters either by geographical position or other factors (coverage area of the node with the most energy). Each of these clusters has a Cluster Head (CH) that collects information from the nodes within it and transmits the information to higher layers or directly to the gateway. The cluster heads normally get rotated periodically for energy saving and network lifespan [6], [9]. Decentralized Military Sensor Networks (DMSN) can be given as an example for the third architecture. In this approach, which is especially important for military applications, there is no single central control point of the network. This structure increases resilience by ensuring that the network continues to operate even in the event of failure of certain nodes or enemy intervention. However, coordination and security management between nodes become more complex [10].

2.2. Military Based Sensor Technologies

The success of military based WSNs in the field of operations directly depends on the type and capabilities of the sensors used. The complex structure of today's battlefields and surveillance requirements necessitate the use of sensors that can perceive many environmental and physical conditions. Figure 2 illustrates several military-grade sensor types commonly used in tactical surveillance, including PIR, infrared and camera traps. The visuals are based on open-access manufacturer resources [11], [12].

Figure 2. Military based sensors (Images adapted from open-access manufacturer resources: ASELSAN, n.d.; Military.eu, n.d.; Naval News, 2021).

2.3. Communication Mechanism and Data Transmission

In military WSNs, the transmission of collected data from the sensor node to the end user (e.g., headquarters) is a critical process. This process is depicted in Figure 3 and generally includes the following steps:

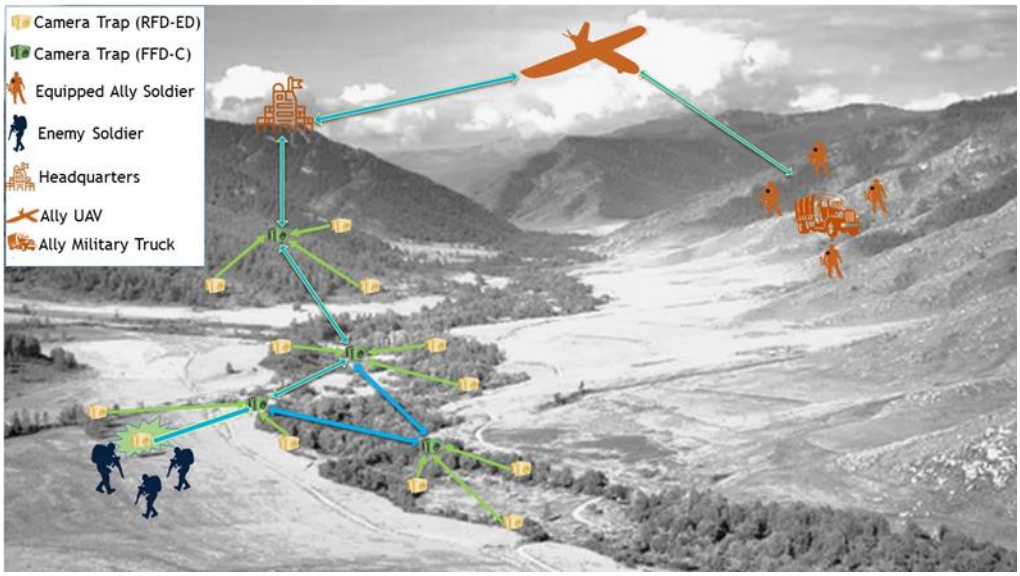

Figure 3. A sample military based sensor network

In the scenario depicted in the figure, when a movement towards the presence of enemy soldiers is detected in the field, this information is first detected by the RFD-ED type camera trap closest to the incident point. The data obtained is transmitted to the nearest FFD-C in line with the hierarchical structure and is preprocessed there. This data is then transferred to a friendly Unmanned Aerial Vehicle (UAV) in a chained manner via the FFD-C nodes at the upper levels of the network. The UAV provides instant situational awareness by transmitting this data to both the headquarters and the friendly military units and military vehicles stationed in the field. That is to say, although the data flow is generally upward (uplink) from the sensors, downwards (downlink) communication from the central units to the nodes may also be required for purposes such as network management, node querying or tasking.

In the context of this scenario, the most important advantages of this structure include energy efficiency, mission-based data routing, event-driven information dissemination and wide area coverage capability. In addition, thanks to the wireless communication established via the UAV, both long-distance communication is provided and rapid decision-making of units in the field is supported.

2.4. Data Processing Strategy

Processing of raw sensor data within the network is important in terms of reducing communication load, saving energy, reducing latency and obtaining more meaningful information. Data processing can be performed on the node, within the distributed network or on the coordinators within the WSN. Data processing on the node can be defined as the most basic processing level. ED processes the raw data it collects (for example, by filtering temperature information, checking threshold values or performing simple event detection) to reduce the amount of data to be sent. This significantly reduces energy consumption, but complex analyses cannot be performed due to the limited processing power and memory of the node. In the distributed in-network data processing process; Data is processed with the cooperation of multiple nodes within the network. For example, cluster heads can aggregate and summarize data from nodes in their own clusters, or neighboring nodes can exchange information for

tasks such as location determination. This allows for more complex analyses, but has the disadvantages of coordination and additional communication load. In the data processing process performed on the coordinators, data is collected in more capable units such as gateways or coordinators and subjected to more comprehensive analyses. Here, data fusion techniques are used to combine information from different sensors or nodes, check consistency, and obtain more reliable results. Data is processed here for the last time before being sent back to the access channel [2], [3], [6]. Effective data processing strategies are critical to extend the life of the network, use bandwidth efficiently, and provide timely, accurate information to decision makers.

3. Applications And Taxonomy of WSNs In Military Operations

Military applications of WSNs can be classified into two main categories: operational and functional perspectives.

Classification According to Operational Scenarios:

- Battlefield Applications (Wide area surveillance, enemy tracking).
- Urban area operations (Building clearance, force protection).
- Non-combat operations (Peacekeeping, disaster relief, environmental monitoring, etc.).
- Force Protection and Base Security (Perimeter monitoring, infiltration detection) [3], [6], [7].

Classification According to Functionality:

- Reconnaissance and Surveillance (Battlefield surveillance, border security, intrusion detection).
- Target Detection, Identification and Tracking (Enemy movement, vehicle/personnel tracking).
- Battlefield Monitoring (Weapon fire, explosion detection, friendly forces health/location tracking).
- Environmental Sensing (CBRN-P detection).
- Logistics and Asset Management (Ammunition/equipment tracking).
- Special Applications (Anti-Submarine Warfare, Self-Healing Mines, Navigation Assistance) [3], [5], [6].

A summary of these application areas, along with the primary sensor types, key advantages, and operational limitations, is presented in Table 1.

Table 1. Application fields of military WSNs: sensor types, advantages, and limitations

Application Area	Primary Sensor Types	Key Advantages	Operational Limitations
Battlefield Surveillance & Target Tracking	Acoustic, Seismic, Magnetic, RADAR, UAV Cameras	Real-time enemy detection, 24/7 continuous monitoring of large areas, significantly minimizes risk to personnel	High bandwidth requirements for UAV video transmission; Line-of-Sight (LoS) losses in rugged terrains or high winds
Perimeter & Border Protection	Passive Infrared (PIR), Camera Traps, LiDAR, Acoustic	Early detection of infiltrations; enabling autonomous warning systems and automated drone routing mechanisms	High false-positive rates triggered by wild animals or extreme weather conditions (e.g., fog, sandstorms)
Connected Soldier & Health Monitoring (IoBT)	Wearable Biometric Sensors (Heart rate, SpO2, EEG, Body Temperature)	Real-time tracking of vital signs; supports rapid medical evacuation decisions (MEDEVAC) and enhances tactical coordination	Strictly limited battery life of wearables; severe risk of enemy eavesdropping on sensitive health and location data
CBRN-P Threat Detection	Chemical/Biological Gas Sensors, Radiological Particle Detectors	Remote detection of lethal toxins without human exposure; facilitates instant tactical evacuation planning	Rapid hardware degradation in harsh combat environments (dust, explosions); necessitates frequent calibration
Logistics & Asset Management	RFID, GPS-enabled trackers, Motion sensors	Efficient tracking of ammunition and vehicles; reduces the risk of friendly-fire incidents	Relies heavily on continuous connectivity; highly vulnerable to GPS spoofing or signal denial

4. Military WSN Requirements and Challenges

The successful deployment and operation of WSNs in military environments brings much more challenging and unique requirements compared to civilian applications. The basic operational, network-based, security and other challenges that WSNs must meet can be generalized in light of the surveyed literature as follows;

4.1. Operational Challenges and Requirements

Deployment: The dynamic nature of military operations requires WSNs to be deployed quickly and appropriately. Nodes can be deployed manually before the operation, or by air (aircraft, UAV) or rocket launchers during conflict or in hard-to-reach areas. This requires the nodes to be physically

rugged. After deployment, it is critical that nodes quickly recognize their neighbors and form a self-organizing (ad-hoc) network [2], [4], [10].

Scalability and Coverage: The scale of military operations is variable. In most scenarios, the area to be covered by the network can be between 5-20 km² and the number of nodes needed is usually expressed in hundreds, which is different from networks of thousands of nodes assumed in some academic studies [2], [3], [6]. While the communication distance between nodes can usually be assumed to be around 250-500 meters, in some cases ranges exceeding 1 km may be needed [2]. The network must be scalable to effectively cover the area required by the mission [3], [6].

Lifetime and Energy Efficiency: Sensor nodes usually have limited battery power and military missions can last for days or even months [2], [6]. Therefore, it is vital that nodes and network protocols are energy efficient. In multi-hop communication, the energy hole problem (EHP), illustrated in Figure 4, is a serious problem where nodes close to the gateway (sink) run out of energy faster due to the increased data transmission load, shortening the network lifetime [9]. Strategies such as clustering, sleep-wake mechanisms, and balanced routing have been developed to alleviate this problem [9].

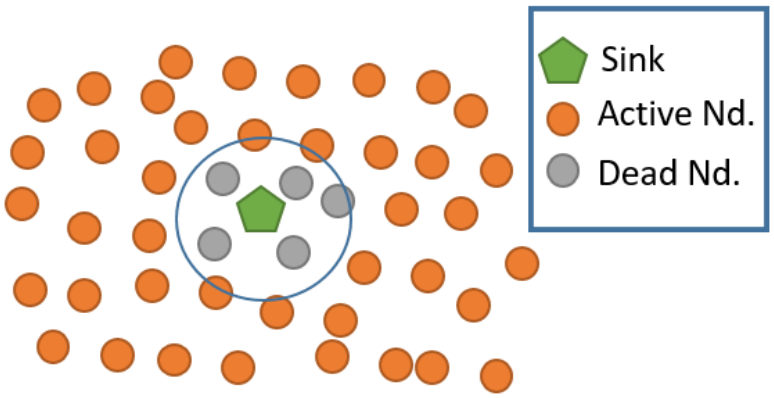

Figure 4. Energy hole problem

Stealth: In military operations, WSN nodes must remain undetected by the enemy. This requires both the nodes to be physically small, camouflaged, and compatible with the environment, and to leave a low electromagnetic signature, making them difficult to detect electronically [2], [6].

4.2. Network Challenges and Requirements

Robustness: Military operational environments are hostile; nodes can fail due to environmental factors, accidents, or enemy action. The network is designed to withstand single node failure or disconnection (fault tolerance) and be resilient to outages [3], [4].

Reliability: It is essential that critical intelligence or early warning data is delivered to central units without loss and on time. Network protocols must have mechanisms to guarantee data transmission [2], [6].

Node Localization: In order for the collected data to be meaningful (e.g., determining the location of a threat), the location of the sensor node collecting the data must be known. Integrating GPS into all nodes is not practical due to reasons such as cost, energy consumption, and not working in every

environment (e.g., indoors, forested areas). Therefore, there is a need for energy-efficient localization algorithms that estimate the location of other nodes using a limited number of reference (anchor) nodes and are robust to environmental noise [13].

Routing: Data must be delivered to the destination (usually the gateway) in the most efficient way within the network. Military WSN routing protocols must be energy-efficient, secure, dynamic (adapting to changing topology), robust (resisting to connection failures), and able to meet the latency requirements of the mission [2], [6], [10].

4.3. Security Challenges and Requirements

Military WSNs are inherently vulnerable to hostile interference, and security is one of the top priorities:

Confidentiality, Integrity, Authentication: Preventing unauthorized reading of transmitted data (confidentiality - encryption), ensuring that data has not been altered during transmission (Integrity), and verifying the identities of communicating nodes (Authentication) are basic security requirements [2], [6], [10].

Jamming Resistance: The network must be resilient to adversary attempts to disrupt communications by deliberately disrupting radio frequencies. Techniques such as frequency hopping or direct sequence spread spectrum can be used [2], [3], [6].

Specific Attacks: The enemy can perform various attacks to disrupt the operation of the network: Precautions should be taken against attacks such as spoofing the node identity, misleading the network with fake identities (Sybil), misrouting packets (Misrouting), swallowing packets (Blackhole/Sinkhole), delaying or replaying packets (Replay), manipulating traffic with wormhole [2], [6].

Tamper-proofing: The enemy should be prevented from obtaining sensitive information (cryptographic keys, collected intelligence, etc.) from a node that has been physically compromised. This may require physical protection and data deletion mechanisms [2], [4].

Denial of Service (DoS): Resilience is important against attacks that aim to render the network unserviceable by consuming network resources or blocking communication.

Secure Deployment and Key Management: Securely locating nodes and securely creating, sharing, and handling cryptographic keys, especially for large distributed networks, is a significant challenge [2], [6], [10].

Intrusion Detection: There needs to be a mechanism to detect malicious nodes or attacks by identifying anomalous activity or known attack patterns inside the network. Machine learning and artificial intelligence-based intrusion detections show good promise here [8], [10].

4.4. Other Challenges

Physical Constraints: Military applications generally require nodes to be small in size, lightweight, low in power and low in cost. They are also expected to be rugged in harsh environmental conditions [2], [3], [4].

Heterogeneous Sensor Integration and Data Fusion: Efficiently combining data from different types of sensors (acoustic, seismic, IR, etc.) provides more accurate and reliable situational awareness, but is technically challenging because of complexity [3], [6].

Lack of Standards: The lack of generally accepted protocols and standards for military WSNs hinders interoperability between different systems and makes development difficult. Standards developed for critical infrastructures can be partially guiding [1].

Considering the various challenges and constraints discussed in this section, a summary of the primary issues in military WSNs and their corresponding modern solutions is provided in Table 2.

Table 2. Primary challenges in military WSNs and proposed state-of-the-art solutions

Challenge Category	Specific Impact in Battlefield Environment	Proposed Modern Solutions
Energy Hole Problem (EHP) & Limited Battery	Rapid depletion of nodes near the sink causes severe network partitioning and total loss of communication.	UAV-assisted mobile sinks and relays [14]; Corona-based layer clustering [6]
Latency & Bandwidth Constraints	Inability to transmit high-definition raw data (from cameras/radars) to headquarters due to severely congested tactical links.	Edge AI integration for local data processing at cluster heads, transmitting only actionable intelligence [15], [16].
GPS Denial & Localization Errors	Adversarial GPS spoofing or jamming leads to misguiding artillery fire and friendly troop movements.	GPS-free localization using bio-inspired optimization methods [9]; Landmark-based localization (LanBLoc) integrated with Extended Kalman Filter (EKF) for secure troop navigation [17]
Signal Jamming & Electronic Warfare (EW)	Blocked radio frequencies render sensor nodes completely "deaf and blind", cutting off critical early warnings.	Deep Reinforcement Learning (DRL) for autonomous frequency hopping [18], [19]; Low Probability of Intercept (LPI) waveforms [2], [20].
Data Privacy & Routing Attacks	Enemy eavesdropping on sensitive troop data or manipulating network topology via Sybil/Blackhole attacks.	Federated Learning (FL) for privacy-preserving model training [21]; Blockchain-based secure routing architectures [10]

5. Recent Developments and Proposed Solutions

These challenges posed in the above section have led scholars to come up with innovative solutions to increase the reliability, lifetime and efficiency of military WSN systems. In recent literature, unprecedented advancements have been made, especially in the areas of energy efficiency, security,

node placement and data analysis. This section discusses the main solution approaches proposed in recent studies in the bibliography.

5.1. Solution Proposals for the Energy Hole Problem (EHP)

The Energy Hole Problem (EHP), which occurs when nodes close to the gateway (sink) are overloaded and consume their energy rapidly, is one of the main problems that limit the lifetime of WSNs. To address this problem, Behera & Mohapatra proposed a cluster model for WSN based on corona. In this model, the network is logically divided into different coronas (layers) and the Cluster Head (CH) selection is done by prioritizing the nodes in the outer coronas which are far from the gateway. In this way, the routing load of the nodes close to the gateway is reduced. In addition, a sleep-wake mechanism is integrated that allows the nodes to go to sleep mode when their energy levels fall below a certain threshold. It is stated that this approach significantly increases the network lifetime and stability compared to traditional protocols such as LEACH and SEP in both homogeneous and heterogeneous networks.

5.2. Secure Routing in Decentralized Military Networks (DMSN)

The hostile and dynamic nature of military environments demands secure and robust routing protocols, especially in decentralized military sensor networks (DMSNs). Traditional blockchain solutions are generally designed for static networks and cannot cope with the dynamism of DMSNs. Rajasoundaran et al. suggested a new solution called GAN-based Blockchain framework for Secure Routing (GBCRP) to mitigate this drawback. In this framework: Instead of fixed chains, temporary blockchains are used that are created on demand and can adapt to changes and disconnections in the network. A distributed Intrusion Detection System (IDS) based on Generative Adversarial Networks (GAN) integrated into each node analyzes network traffic, detects attacks and anomalous behaviors, and alerts the blockchain protocol. AODV protocol is used for basic routing, but it is strengthened with Digital Signature Algorithm (DSA) for node authentication and Advanced Encryption Standard (AES) for data privacy. The integration of these components aims to provide solutions to the challenges of the DMSN environment by creating a routing mechanism that is both dynamic and secure.

5.3. Advanced Node Localization Techniques

Accurate determination of node locations is critical for the meaningfulness of the collected data. Optimization algorithms are widely used to improve localization accuracy, especially when GPS is unavailable or costly. However, some algorithms, such as the Bat Optimization Algorithm (BOA), can tend to get stuck in local optima. Mohar et al. proposed two new variants of the original BOA to overcome this problem and improve localization performance. BOA Variant 1 uses an improved global search strategy to increase exploration capability, scanning a larger portion of the solution space. BOA Variant 2 uses an improved local search strategy to improve exploitation capability, searching the area around the current best solution more effectively. Simulations have shown that these two variants converge faster and successfully localize more nodes with less localization error compared to the

original BOA and other optimization algorithms such as PSO, FA, GWO. In particular, BOA variant 2 has been reported to exhibit superior performance in terms of both computational time and accuracy.

Although the bio-inspired optimization algorithms greatly reduce the mean value of the localization errors without introducing any additional costs to the system in terms of hardware requirements, there are several drawbacks that should be noted about their use in practical settings. For example, even though these algorithms are designed for GPS-denied environments, achieving high accuracy still inevitably relies on a subset of GPS-enabled anchor nodes as reference points. Deploying a large number of such nodes in a conflict area will cause both higher expenses and much higher chances of complete system blinding owing to the EW capabilities of the adversary, such as spoofing or jamming the GPS signals. Therefore, deploying these algorithms in combat zones requires a rigorous trade-off between localization precision and the survivability of anchor nodes.

5.4. Artificial Intelligence-Assisted Monitoring and Analysis

In military surveillance applications, the interpretation of visual data (images/videos), especially from WSNs equipped with cameras, can be difficult due to factors such as environmental noise, bad weather conditions or low light. Mahamuni & Jalauddin proposed the use of Deep Learning techniques, especially Convolutional Neural Networks (CNNs), to overcome this challenge. In the proposed system, when a CBRN-P or intrusion sensor (e.g. PIR sensor) triggers an event, the camera module is activated and the resulting images are sent to a central server for analysis. The CNN model running on the server is trained to detect and track multiple objects (e.g. people, vehicles, animals) in the images with high accuracy. It has been reported that this approach provides high detection and classification accuracy (around 92%) and satisfactory object tracking efficiency on test images captured under different conditions.

While the centralized approach to CNN-based image processing promises high theoretical accuracy, the practical relevance of such a technique in combat situations is questionable. Even under the framework of the event-driven architecture when transmissions occur only when necessary, transferring high-definition raw images and/or video streams from camera-based WSN nodes to the centralized command server requires considerable bandwidth and a continuously stable connection. Under the challenging conditions of the field, however, the tactical network connections tend to be intermittent, restricted in terms of bandwidth, and vulnerable to being compromised by the adversary through signal interference or jamming. In addition, constantly sending large amounts of visual data will quickly drain the already limited energy reserves of the deployed sensor nodes. Thus, for AI-based image recognition to become feasible on the battlefield, future approaches to the problem need to rely on the Edge AI framework that enables image analysis to occur on-site, with only relevant information being sent back to headquarters.

5.5. Emerging Paradigms: Internet of Battlefield Things (IoBT), Edge AI, and Advanced Tactical Networks

Other than traditional architectures, current literature ranging from 2023 to 2025 indicates a shift in paradigms towards Internet of Battlefield Things (IoBT) and Military Internet of Things (MIoT) networks. IoBT network expands the functionalities of conventional WSNs in that it connects sensors, soldiers, autonomous systems, weapon systems, and wearable devices within a single smart battlefield communication network (Pióro et al., 2024; Kufakunesu et al., 2025; Rettore et al. 2025). Under this framework, UAV-enabled WSNs are receiving considerable attention. UAVs are now extensively used as mobile sinks and relay nodes to help collect information dynamically from ground-based sensors, and therefore overcome the Energy Hole problem and keep the communication link active in harsh terrain conditions [14], [22], [23], [24]. Despite improving the coverage and lifetime of UAV-assisted WSNs, they raise additional issues such as trajectory planning and resistance against electronic jamming. While the use of UAVs as mobile sinks theoretically resolves the energy hole problem on the ground, it critically shifts the energy bottleneck to the aerial nodes due to their strictly limited onboard battery capacities and flight times. Furthermore, in rugged and windy battlefield terrains, the angular instability of UAVs severely degrades the performance of high-speed links, making reliable communication highly challenging without advanced mitigating technologies like Modulating Retro-Reflectors (MRR). Therefore, practically deploying UAV-assisted WSNs in frontline combat requires a delicate trade-off between aerial endurance, stealth, and payload weight.

In order to solve the issue of latency and bandwidth constraints due to large transmission of raw data from the battle zone to centralized command stations, Edge AI and Federated Learning (FL) become revolutionary tools. With the help of Edge AI, machine learning models can be deployed in cluster heads or sophisticated sensors to process data locally and thereby make decisions promptly [15]. Moreover, FL helps train a model among a number of nodes by making them work together without exchanging any raw and confidential information [21], [25]. However, it should be noted that, while federated learning provides excellent data security and safe network management in the context of a tactical network, computational and memory overhead remain a major obstacle for WSN nodes powered only by batteries. Moreover, the applicability of FL in highly contested military environments may be constrained by its dependence on iterative parameter exchanges, which can be vulnerable to intermittent connectivity and jamming. Although techniques such as top-k gradient sparsification have been proposed to alleviate communication overhead, the communication-efficiency trade-off remains a significant challenge. In comparison, Edge AI is often preferred for latency-sensitive and highly dynamic tasks such as real-time threat recognition and autonomous target engagement, whereas FL may offer advantages in rear-echelon intelligence and planning applications where privacy preservation is critical and communication links are comparatively stable.

Lastly, survivability in military WSNs mainly depends on effective communication. Recently, there's been a focus on anti-jamming methods using reinforcement learning. These let nodes switch

frequencies or power up their transmissions when threats threat has been detected [18], [19]. When combined with AI-powered intrusion detection systems (IDS), networks become way better at telling real node faults apart from intentional attacks like Sybil or blackhole [10], [25]. But these security methods need regular updates to keep up with evolving threats. Evaluating AI-driven defenses shows some major issues. For example, DRL and advanced IDS systems typically need lots of training data and computing power. This can be tough to maintain in dynamic nature of battlefields where resources are limited. Furthermore, while these systems often do promising performance in tests, telling smart jamming apart from channel impairments isn't always easy. Mistakes in detection can set off false alarms and waste energy on unnecessary countermeasures. So, for true resilience in combat situations, we need security solutions that not only spot threats effectively but also don't overload the system.

5.6. Other Approaches and Techniques

Apart from the approaches discussed in previous sections, other research directions have also played a significant role in developing military WSNs. One key area focuses on making secure routing protocols, where security mechanism is built right into how data routes through the network. Some examples include Ariadne, SAODV, SRP, and SEAD which aim to protect routing operations against various network attacks [26].

Another area of active research focuses on trust management models. Trust management models monitor the behavior of nodes in the network over time and compute a trust value for that node based on its observable actions. This information can be used as part of the routing decision-making process to reduce the effects of a malicious or compromised node or a non-cooperative node, which improves the overall reliability of the network.

Furthermore, fusion techniques for gathering and correlating sensor data have been widely studied in military WSN applications. These methods improve confidence and reliability of the information gathered from many different sensors or platforms when combined with data obtained using other disparate sensing mechanisms; thereby, providing a more complete picture in order to obtain superior situational awareness under highly dynamic conditions of modern battle scenarios by addressing the deficiencies present in the use of single sensor systems.

These recent advances propose different and promising solutions to military WSN problems. These attempts of improving energy efficiency, security guarantee, location accuracy and intelligent data analysis will further improve the prospects of WSNs in the military domain.

Table 3 shows a comparative summary of the recent studies, their proposed methodologies, key strengths and major limitations.

Table 3. Comparative analysis of recent studies and approaches in military WSNs

Author(s) & Year	Focused Problem	Proposed Methodology / Architecture	Key Strengths (Advantages)	Major Limitations (Critical Analysis)
Sapkota & Madria (2024)	Troop Navigation and Node Localization in GPS-Denied Environments	Landmark-based localization (LanBLoc) integrated with Extended Kalman Filter (EKF)	Provides secure, highly accurate point-forward navigation for mobile troops without relying on vulnerable radio-based anchors.	Heavily depends on identifiable physical landmarks and predefined hazard maps; computational filtering requires reliable prior tactical data.
Behera & Mohapatra (2021)	Energy Hole Problem (EHP) and Limited Lifetime in Military Applications	Corona-based layer clustering and Sleep-Wake scheduling mechanisms	Efficiently mitigates the heavy traffic load for nodes near the sink without requiring additional aerial hardware, substantially extending network lifetime.	Existing static layer clustering approaches cannot well adapt to the extreme mobility and unpredictable topological changes of active combat troops.
Wang et al. (2025); Kufakunesu et al. (2025)	High Latency and Bandwidth Bottlenecks in the Tactical Edge	Edge AI architecture for the IoBT	Processes raw data locally, enabling millisecond-level decision-making essential for autonomous weapon engagements and reducing tactical link congestion.	The sensor edge has limited memory and processing power, creating serious bottlenecks for deploying complex AI models in contested environments.
Rajasoundaran et al. (2021)	Data Breaches, Routing Attacks (Sybil/Blackhole), and Anomaly Detection	Fully Decentralized Generative Adversarial Network (FDGAN) and Blockchain-based Secure Routing (GBCRP)	Achieves excellent data privacy and securely isolates compromised nodes/attackers using tamper-proof distributed ledgers and intelligent IDS agents.	Blockchain consensus and continuous attack signature updates introduce significant computational overhead, making it highly susceptible to system failure.

6. Conclusion

Wireless Sensor Networks (WSNs) have a transformative role for modern military operations providing stealthy, cost-effective, and continuous intelligence-gathering capabilities. However, the deployment of WSNs in battlefields is highly constrained by factors such as energy limitations for wireless nodes, GPS signal interference and electronic warfare threats, as discussed in this research. Therefore, it is necessary to deal with several important and critical evaluations for the transition from theoretical models to practical frontline deployments.

It is possible to form a critical analysis of state-of-the-art solutions as follows. Recent trends demonstrate a crucial paradigm shift from classical routing protocols to autonomous AI-Driven architectures. Innovations including corona-based clustering and UAV-powered mobile receivers effectively tackle the Energy Hole Problem (EHP). Similarly, biologically inspired optimization algorithms and the landmark-based Extended Kalman Filters (EKF) enable robust navigation in environments where GPS is unavailable. The practical application of these technologies in active combat involves substantial trade-offs. For example, while the deployment of a dense set of anchor nodes is essential to achieve high positioning accuracy in a combat environment, it inevitably increases the number of radiating elements that can be detected by the enemy. This paradoxically increases network's vulnerability to enemy electronic warfare blinding (e.g., GPS spoofing). UAVs also overcome ground-based energy bottlenecks, but their limited battery/fuel capacities make them highly susceptible to angular instabilities and rapid battery depletion in rugged, high-altitude and windy terrain.

Despite the efficient advances, the literature still has major research gaps. First, sophisticated Deep Reinforcement Learning (DRL) and Intrusion Detection Systems (IDS) incur significant computational and memory overhead, limiting their deployment on battery-powered tactical edge nodes. Second, it is challenging to discriminate between intelligent jamming attacks and complicated channel impairments (e.g., severe multipath fading or shadowing), which can often lead to false alarm and energy-wasting evasive maneuvers. Finally, many of the current secure routing and clustering mechanisms, such as static layer clustering or continuous blockchain consensus, are unable to cope with the extreme mobility, unpredictable topological changes, and intermittent connections of active combat troops.

To fill these gaps, future military sensor networks must seamlessly evolve to the Internet of Battlefield Things (IoBT). Research should focus on ultra-lightweight cryptographic algorithms and advanced energy harvesting techniques for long-term and infrastructure-less operations. Furthermore, the shift from centralized clouds to Edge AI as a computational paradigm will be key to supporting millisecond-level, latency-sensitive tasks such as autonomous target engagement. At the same time, optimization of communication-efficient Federated Learning (FL), e.g., top-k gradient sparsification, will allow distributed nodes to train cyber-threat models securely without saturating tactical bandwidths. Finally, the design of context-aware, self-healing network protocols, integrating Software-Defined

Networking (SDN) and decentralized architectures, will be critical to construct resilient, agile and highly secure military systems for next-generation warfare.

Declarations

Ethical Approval: As this study is a systematic review of existing literature and does not involve any human or animal subjects, ethics committee approval is not required in accordance with the journal's ethical guidelines.

Conflict of Interest: The author declares that there is no conflict of interest regarding the publication of this paper.

Funding: This research received no specific grant from any funding agency in the public, commercial, or not-for-profit sectors.

References

[1] S. Daousis, N. Peladarinos, V. Cheimaras, P. Papageorgas, D. D. Piromalis, and R. A. Munteanu, "Overview of protocols and standards for wireless sensor networks in critical infrastructures," *Future Internet*, vol. 16, no. 1, p. 33, 2024.

[2] M. Winkler, K.-D. Tuchs, K. Hughes, and G. Barclay, "Theoretical and practical aspects of military wireless sensor networks," *J. Telecommun. Inf. Technol.*, no. 2, pp. 37–45, 2008.

[3] M. P. Đurišić, Z. Tafa, G. Dimić, and V. Milutinović, "A survey of military applications of wireless sensor networks," in *Proc. 2012 Mediterranean Conf. Embedded Comput. (MECO)*, 2012, pp. 196–199.

[4] S. B. Prabhu, N. Balakumar, and A. J. Antony, "Evolving constraints in military applications using wireless sensor networks," *Int. J. Innovative Res. Comput. Sci. Technol.*, pp. 2347–5552, 2017.

[5] S. Pragadeswaran, S. Madhumitha, and S. Gopinath, "Certain investigation on military applications of wireless sensor network," *Int. J. Adv. Res. Sci. Commun. Technol.*, vol. 3, no. 1, pp. 14–19, 2021.

[6] T. M. Behera and S. K. Mohapatra, "A novel scheme for mitigation of energy hole problem in wireless sensor network for military application," *Int. J. Commun. Syst.*, vol. 34, no. 11, p. e4886, 2021.

[7] A. Ali, Y. K. Jadoon, S. A. Changazi, and M. Qasim, "Military operations: Wireless sensor networks based applications to reinforce future battlefield command system," in *Proc. 2020 IEEE 23rd Int. Multitopic Conf. (INMIC)*, 2020, pp. 1–6.

[8] C. V. Mahamuni and Z. M. Jalauddin, "Intrusion monitoring in military surveillance applications using wireless sensor networks (WSNs) with deep learning for multiple object detection and tracking," in *Proc. 2021 Int. Conf. Control Autom. Power Signal Process. (CAPS)*, 2021, pp. 1–6.

[9] S. S. Mohar, S. Goyal, and R. Kaur, "Localization of sensor nodes in wireless sensor networks using bat optimization algorithm with enhanced exploration and exploitation characteristics," *J. Supercomput.*, vol. 78, no. 9, pp. 11975–12023, 2022.

[10] S. Rajasoundaran, S. S. Kumar, M. Selvi, S. Ganapathy, R. Rakesh, and A. Kannan, "Machine learning based volatile block chain construction for secure routing in decentralized military sensor networks," *Wireless Netw.*, vol. 27, no. 7, pp. 4513–4534, 2021.

[11] ASELSAN, "Piri100 Passive Infrared Detector," [Online]. Available: https://www.aselsan.com/en/defence/product/2956/piri100. Accessed: May 24, 2025.

[12] Naval News, “Thales creates acoustic shot detector sensor for maritime environment,” May 2021. [Online]. Available: https://www.navalnews.com/naval-news/2021/05/thales-creates-acoustic-shot-detector-sensor-for-maritime-environment/. Accessed: May 24, 2025.

[13] G. Hacioglu and E. Sesli, “Improved RSS based distance estimation for autonomous vehicles,” *Wireless Pers. Commun.*, vol. 125, no. 1, pp. 325–350, 2022.

[14] M. T. Dabiri and M. Hasna, “A novel MRR-UAV based relay with optical network coding: A comparative study with optical IRS and conventional UAV relaying,” *IEEE J. Sel. Areas Commun.*, 2025.

[15] S. Wang, Q. Jia, Y. Wang, and J. Ma, “The application of edge artificial intelligence in the Internet of Battlefield Things,” in *Proc. 2025 4th Int. Symp. Comput. Appl. Inf. Technol. (ISCAIT)*, 2025, pp. 1413–1417.

[16] R. Kufakunesu, H. Myburgh, and A. De Freitas, “The internet of battle things: a survey on communication challenges and recent solutions,” *Discover Internet of Things*, vol. 5, no. 1, p. 3, 2025.

[17] G. Sapkota and S. Madria, “Secure navigation using landmark-based localization in a gps-denied environment,” *arXiv preprint arXiv:2402.14280*, 2024.

[18] S. Goyal, M. Gupta, K. Bhuvaneshwari, P. Saini, K. Yuvaraj, and B. Babitha, “Enhancing Wireless Connectivity Networks Through Intruder Jamming Detection and Localization with Advanced Techniques,” in *Proc. 2025 Int. Conf. Electr. Eng. Inform. (ICEEI)*, 2025, pp. 1–8.

[19] A. Yu, I. Kolotylo, H. A. Hashim, and A. E. Eltoukhy, “Electronic warfare cyberattacks, countermeasures and modern defensive strategies of UAV avionics: a survey,” *IEEE Access*, 2025.

[20] K. Rhee, J. Baik, C. Song, and H.-C. Shin, “LPI radar waveform recognition based on hierarchical classification approach and maximum likelihood estimation,” *Entropy*, vol. 26, no. 11, p. 915, 2024.

[21] X. Zhang et al., “Latency minimization for UAV-enabled federated learning: Trajectory design and resource allocation,” *IEEE Internet Things J.*, 2025.

[22] O. M. Gul and A. M. Erkmen, “Energy-efficient cluster-based data collection by a UAV with a limited-capacity battery in robotic wireless sensor networks,” *Sensors*, vol. 20, no. 20, p. 5865, 2020.

[23] R. A. Nazib and S. Moh, “Energy-efficient and fast data collection in UAV-aided wireless sensor networks for hilly terrains,” *IEEE Access*, vol. 9, pp. 23168–23190, 2021.

[24] G. H. F. Diédié, A. K. Atiampo, and T. N’Takpé, “Sink’s One-Hop Neighborhood Energy Hole Mitigation Scheme for Dense Wireless Sensor Networks,” *J. Commun.*, vol. 18, no. 12, 2023.

[25] L. Bhagyalakshmi, K. Krishnamoorthy, S. F. Waris, and M. Karthiga, “Precise Anomaly Recognition Using Advanced Federated Learning in Resource-Restricted WSN With Unreliable Connections,” *Int. J. Commun. Syst.*, vol. 39, no. 5, p. e70424, 2026.

[26] A. Baradaran, “The applications of wireless sensor networks in military environments,” *Sci. J. Rev.*, vol. 4, no. 4, pp. 55–70, 2015.